REVIEW

Check for updates

Navigating ionic conductivity in MOF electrolytes: addressing measurement pitfalls and performance limits

Zina Deriche, [ID] [a] Sibani Lisa Biswal [ID] [ab] and Stavroula Kampouri [ID] *[abc]

Solid-state batteries promise significant improvements in energy density and safety over conventional liquid-electrolyte systems, yet realizing their full potential hinges on developing solid electrolytes with high ionic conductivity and long-term cycling stability. Metal–organic frameworks (MOFs) have emerged as attractive candidates due to their high porosity, tunability, and structural versatility. However, integrating MOFs into solid-state batteries faces several critical challenges, such as high interfacial resistance, chemical reactivity at electrode–electrolyte interfaces, mechanical brittleness during cycling, and parasitic proton conduction. These issues are compounded by persistent pitfalls in accurately characterizing ionic conductivity, including ambiguities in distinguishing intrinsic Li^+ transport from extrinsic protonic or solvent-mediated contributions and a lack of standardized measurement protocols. In this review, we first explore the interplay between MOF structural features and ion transport mechanisms. Then, we critically assess current strategies to overcome interfacial, chemical, and mechanical barriers, including composite membrane fabrication, defect engineering, and framework design. Finally, we propose best practices for electrochemical impedance spectroscopy (EIS) and cycling tests, emphasizing rigorous controls to decouple intrinsic ion conduction from extrinsic contributions. By addressing material and methodological challenges, this work aims to advance the development and accurate evaluation of MOF-based electrolytes for next-generation energy storage applications.

[a]*Department of Chemical and Biomolecular Engineering, Rice University, Houston, TX 77005, USA. E-mail: Stavroula.Kampouri@rice.edu*

[b]*Rice Advanced Materials Institute (RAMI), Rice University, Houston, TX 77005, USA*

[c]*Chemistry Department, Rice University, Houston, TX 77005, USA*

Zina Deriche is a PhD candidate in Chemical and Biomolecular Engineering at Rice University. She earned her B.S. in Chemical Engineering with a minor in Environmental Engineering from the University of Minnesota in 2023. Her doctoral research focuses on the design and application of metal–organic frameworks (MOFs) for solid-state battery technologies. Her work aims to advance safer, high-performance energy storage systems, bridging materials design with practical electrochemical applications.

Zina Deriche

Dr Sibani Lisa Biswal is the William M. McCardell Professor and Chair of the Department of Chemical and Biomolecular Engineering at Rice University in Houston, Texas. She has a B.S. in chemical engineering from Caltech and a PhD in chemical engineering from Stanford University. She leads the Soft Matter Engineering Laboratory, where she focuses on establishing connections between the rheological behaviour of particulate and multiphase systems and the underlying physics governing colloidal assemblies, surfactant stabilization related to foams and emulsions, and the development of inorganic–organic battery composites.

Sibani Lisa Biswal

33012 | *J. Mater. Chem. A*, 2025, **13**, 33012–33033

This journal is © The Royal Society of Chemistry 2025

1   Introduction

Since the commercialization of rechargeable batteries in the 1990s, the global demand for energy storage has grown exponentially.[1,2] This surge has driven relentless efforts to enhance battery performance, particularly as the urgency to transition toward sustainable energy storage technologies intensifies amid escalating climate challenges.[3,4] Addressing this demand requires innovations that deploy eco-friendly solutions while maximizing safety and efficiency.[3,5] Solid-state batteries represent a promising approach in this pursuit.[5,6] A solid-state battery consists of an industry-standard cathode (such as a sulfide or oxide), a solid electrolyte (usually a ceramic or polymer), and an anode – often Lithium (Li) metal or silicon.[7,8] Unlike conventional lithium-ion batteries that use flammable liquid electrolytes, solid-state electrolytes offer improved safety, higher energy density, and longer lifespans.[6,9,10] To realize their full potential, however, solid electrolytes must achieve ionic conductivities comparable to those of their liquid counterparts, which typically range from 10^{-3} to 10^{-2} S cm^{-1} at room temperature.[11] Meeting this benchmark is essential to establishing solid-state batteries as a transformative technology for next-generation energy storage.

The principal challenge in solid-state electrolytes lies in ion transport, as ion diffusion in solids is generally much slower than in liquids.[12,13] In solids, ions typically move *via* a hopping mechanism between fixed sites in a rigid lattice.[14–16] This process is inherently less efficient than free ion transport in liquids, where the absence of a fixed lattice allows for greater mobility.[14–16] The material's structure, defect density, and ionic species play a critical role in determining ion diffusion rates.[14,16] The most common materials for solid-state electrolytes are ceramics and polymers.[6,7] Ceramics generally offer high ionic conductivity but are brittle and require energy-intensive processing.[17,18] On the other hand, polymers provide suitable mechanical flexibility, but often suffer from limited conductivity and chemical stability.[17,18] These limitations have prompted the exploration of alternative materials.[16,18,19]

Metal–organic frameworks (MOFs) are at the forefront of materials science, owing to their remarkable porosity, tunable structures, and versatile functionalities.[20–22] Composed of metal nodes coordinated to organic linkers, MOFs form highly porous crystalline networks that can be tailored at the atomic level.[20] Their high internal surface areas, along with their tunable pore size and chemical composition, make them promising for various applications, including energy storage.[16,23–25] Recent advances in ionically conductive MOFs have highlighted their potential as solid-state battery electrolytes.[16,23,25–27] However, achieving efficient ionic conductivity, particularly for lithium ions (Li$^+$), remains challenging, as few examples demonstrate both long-term stability and high conductivity.[16,23,28] This limitation reflects a still-evolving understanding of ionic dynamics within MOFs, including the influence of framework flexibility, pore environment, ion–framework interactions, and guest molecule behavior – all of which must be controlled to enable practical performance in solid-state devices.[16]

In this context, several reviews, such as the one by Kharod *et al.*, have thoughtfully examined strategies to enhance ionic conductivity in MOFs through structural modifications and functionalization.[16] Similarly, Wei *et al.* and Sadakiyo *et al.* have highlighted significant advancements in lithium-ion and proton conduction, respectively.[29,30] Building on these foundational contributions, this review turns its focus to areas that remain less thoroughly addressed, including ongoing pitfalls in the field, such as ambiguities in conductivity characterization, limited standardization in measurement practices, and the need for more systematic design strategies to improve ion transport performance. Emphasis is placed on challenges such as interfacial resistance and structural design limitations, which continue to hinder practical implementation. By addressing these often-overlooked issues and providing targeted strategies to overcome them, this work aims to complement existing literature, contributing to the advancement of MOFs as viable next-generation solid electrolytes, capable of supporting safer, high-capacity energy storage aligned with global sustainability goals.

Stavroula (Alina) Kampouri is a tenure-track Assistant Professor of Chemical and Biomolecular Engineering at Rice University, with a joint appointment in the Department of Chemistry. She earned her B.S./M.S. in Environmental and Chemical Engineering at the Technical University of Crete (TUC) in 2015. In 2020, she completed her PhD in Chemistry and Chemical Engineering in the laboratory of Professor Berend Smit, under the

Stavroula Kampouri

co-supervision of Dr Kyriakos Stylianou at the Swiss Federal Institute of Technology Lausanne (EPFL). Her doctoral research focused on designing photocatalytic systems based on metal–organic frameworks (MOFs) for hydrogen production and water remediation. Following this, she joined the research group of Professor Mircea Dincă in the Department of Chemistry at the Massachusetts Institute of Technology (MIT) as a Postdoctoral Research Fellow to work on the design of conductive MOFs. Her research focuses on designing functional porous materials, particularly MOFs, and exploring structure–property relationships for applications in light-driven catalysis and solid-state batteries.

2   Proton interference in MOFs: impact on ionic conductivity measurements

While much of the focus in MOF-based electrolytes has centered on ion transport mechanisms and structural design, proton interference presents an equally critical challenge in accurately assessing their ionic conductivity. Due to their high porosity

This journal is © The Royal Society of Chemistry 2025

J. Mater. Chem. A, 2025, **13**, 33012–33033 | **33013**

and often hygroscopic nature, MOFs readily absorb moisture and guest vapors, leading to unintended proton conduction. This parasitic effect masks the intrinsic transport behavior of target ions, such as Li^+, making it difficult to accurately determine a material's actual ionic conductivity behavior. This section examines the role of environmental exposure, particularly to water and other solvent vapors, in inflating apparent conductivity through unintended proton transport. It is organized into three subsections: (2.1) Mechanistic understanding of ionic conductivity introduces foundational equations governing ion transport, with a focus on the distinctions between vehicle, Grotthuss, and vacancy-based conduction mechanisms; (2.2) Proton interference and extrinsic effects in MOF-based electrolytes examines sources of error that can lead to inaccurate conductivity measurements due to unintended proton and solvent contributions; and (2.3) Distinguishing intrinsic *vs.* extrinsic ionic conductivity presents experimental evidence of humidity-induced quasi-solid-state ion conduction and outlines strategies to distinguish and mitigate extrinsic proton interference. Together, these subsections provide a rigorous framework for understanding and controlling proton interference, helping ensure that reported conductivity values for MOF-based electrolytes accurately reflect their intrinsic ion transport properties.

2.1 Mechanistic understanding of ionic conductivity

Ionic conduction in extended solids involves the migration of ions through a rigid lattice. Unlike in liquids, where ions move freely, solids typically require structural defects, such as vacancies or interstitial ions, to facilitate ion diffusion. Ionic conductivity in solids is quantitatively described by key equations linking ion dynamics to measurable transport properties. We begin by presenting the fundamental equations that describe ion transport and electrical conductivity, establishing the basis for analyzing ion transport mechanisms.

Ionic conductivity (σ_i), typically reported in S cm^{-1}, is defined by the product of charge carrier density (c_i) in cm^{-3}, ion charge (q_i) in C, and mobility (μ_i) in cm^2 V^{-1} s^{-1}:

$$\sigma_i = c_i q_i \mu_i \tag{1}$$

Ion mobility is related to the diffusion coefficient (D_i) cm^2 s^{-1} through the Nernst–Einstein relation:

$$\mu_i = \frac{q_i D_i}{k_B T} \tag{2}$$

where k_B is the Boltzmann constant in J K^{-1}, and T is the temperature in K.[31] The diffusion coefficient follows an Arrhenius-type dependence:

$$D_i = D_0 e^{-E_a/k_B T} \tag{3}$$

Here, the pre-exponential factor (D_0) in cm^2 s^{-1}, reflects intrinsic lattice dynamics, and the activation energy (E_a) in J, is the barrier ions must overcome to hop between vacancy sites (Fig. 2III and IV).[16,31] The transference number (t_i) quantifies the ionic contribution to total conductivity:

$$t_i = \frac{\sigma_i}{\sigma_i + \sigma_e} \tag{4}$$

where σ_e is the electronic conductivity.[31] For an ideal electrolyte, $t_i \approx 1$, indicating negligible electronic leakage ($\sigma_e \lesssim 10^{-11}$ S cm^{-1}).[16]

The ionic conductivity of an extended solid is typically measured using electrochemical impedance spectroscopy (EIS) and calculated using the following equation:

$$\sigma_i = \frac{l}{A R_b} \tag{5}$$

where the bulk resistance (R_b) in Ω is obtained from the low-frequency intercept of the Nyquist plot (Fig. 1). This equation allows direct calculation of the ionic conductivity from the measured thickness of the material (l) in cm and cross-sectional area (A) cm^2.[32] This widely used method assumes that R_b reflects the intrinsic resistance of the extended solid. In practice, however, extrinsic contributions such as contact resistance, cell geometry, and electrode interfaces can influence the measured impedance. Although typically minor, these effects should be minimized and, when possible, the uncompensated resistance should be accounted for during data interpretation.

Designing efficient ion conductors relies on minimizing activation energy, which is primarily governed by structural factors, such as the electrolyte lattice geometry, bond polarizability, and vacancy density – all of which govern ion migration barriers. Unlike conventional solid electrolytes, which depend almost exclusively on single-ion hopping or concerted-ion diffusion through a dense lattice, MOFs enable a hybrid set of pathways that blend liquid- and solid-state features.[33,34] They are typically activated by soaking in liquid electrolytes, allowing the solvent and ionic species to infiltrate the pores.[16,35] Upon drying, the solvent may partially evaporate or remain confined within the pores, resulting in a dry, solid-state material rather than a suspension. MOFs can facilitate four distinct ion transport mechanisms, either individually or in combination (Fig. 2). (I) The vehicle mechanism involves ions being carried by mobile species, typically resulting in activation energies (E_a) greater than 0.4 eV (Fig. 2I).[36–38] (II) The Grotthuss mechanism enables ion transport through hopping between fixed, solvated sites such as H_3O^+, NH_4^+ in a relay-like fashion, generally yielding E_a values below 0.4 eV (Fig. 2II).[36,38,39] (III) Single-ion diffusion occurs as individual cations hop between lattice vacancies (Fig. 2III),[16,34,40] and (IV) concerted-ion diffusion involves the synchronous movement of multiple ions, transiently lowering the energy barrier and enabling conduction with E_a values as low as 0.2 eV (Fig. 2IV).[34,41–43] Therefore, targeting Grotthuss and concerted diffusion modes is essential for high-performance MOF-based ionic conductors. Identifying the dominant transport pathway requires comprehensive analysis, including measurements of cation transference numbers and investigation of ion and solvent dynamics using spectroscopic techniques such as solid-state NMR. Ideally, these experimental insights should be supported by computational modeling to enable a reliable assignment of the operative mechanism.[16,33]
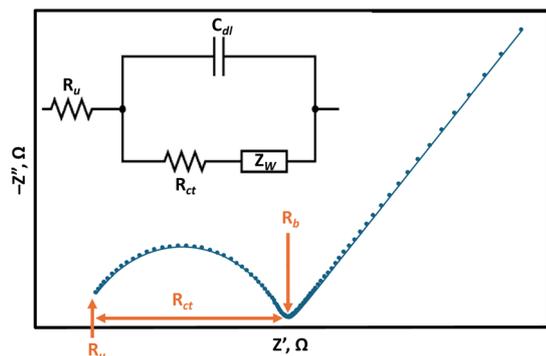
33014 | *J. Mater. Chem. A*, 2025, **13**, 33012–33033

This journal is © The Royal Society of Chemistry 2025

Fig. 1 Nyquist plot and equivalent circuit model representing ion transport and interfacial processes in a solid-state electrolyte system. The circuit consists of an uncompensated resistance (R_u), a parallel combination of the double-layer capacitance (C_{dl}), charge transfer resistance (R_{ct}), and Warburg impedance (Z_w) accounting for semi-infinite ion diffusion. The plot features a depressed semicircle at intermediate frequencies corresponding to $R_{ct}\|C_{dl}$, followed by a low-frequency tail arising from Z_w. The intercept at high frequencies represents R_u, while the total semicircle width corresponds to R_{ct}. R_b denotes the real axis projection of bulk impedance contributions. R_b is the value used to calculate ionic conductivity in eqn (5) of Section 2.1.

2.2 Proton interference and extrinsic effects in MOF-based electrolytes

Accurately assessing ionic conductivity in MOF-based electrolytes requires distinguishing between intrinsic and extrinsic ion transport mechanisms. Although MOFs can be designed to facilitate the conduction of specific ions (*e.g.*, Li$^+$), their highly porous and often hygroscopic nature makes them susceptible to absorbing ambient vapors, particularly water. This uptake of external molecules can introduce unintended proton conduction pathways that may dominate the measured ionic conductivity, especially under humid or elevated-temperature conditions. As a result, materials that appear to exhibit high ion conductivity may, in fact, function as quasi-solid-state conductors, where ion transport is governed by extrinsic factors, rather than the MOF.[44] This subsection examines studies illustrating how uncontrolled environmental exposure can inflate performance metrics, obscure the identity of charge carriers, and ultimately misrepresent a MOF's suitability as an electrolyte.

A clear example of this interference was reported by Brus *et al.*, who investigated MIL-53 loaded with lithium metallacarborane salt (Li$^+$[Co(C$_2$B$_9$H$_{11}$)$_1$]$^-$ or LiCoD).[45] MIL-53 is a "breathing" MOF that can reversibly adopt narrow-pore and open-pore conformations. When loaded with LiCoD, MIL-53 showed an intrinsic Li$^+$ conductivity on the order of 10^{-6} S cm^{-1} at 100 °C. However, at 75% relative humidity (RH), the conductivity increased by nearly three orders of magnitude ($\sim 10^{-3}$ S cm^{-1} at 100 °C). This dramatic enhancement is attributed to water absorption acting as a secondary dopant, which likely formed a percolating network of H$^+$ or H$_3$O$^+$ within the pores. The presence of these fast-moving polar protic charge carriers significantly boosted the overall conductivity. Consequently, MIL-53, intended to be a single-ion Li$^+$ conductor, functioned as a mixed conductor under ambient conditions, with extrinsic proton transport dominating the ion conduction behavior.

Temperature can further exacerbate proton conduction in MOF-based systems, particularly in the presence of Li salts. Sarango-Ramírez *et al.* demonstrated this in a two-dimensional
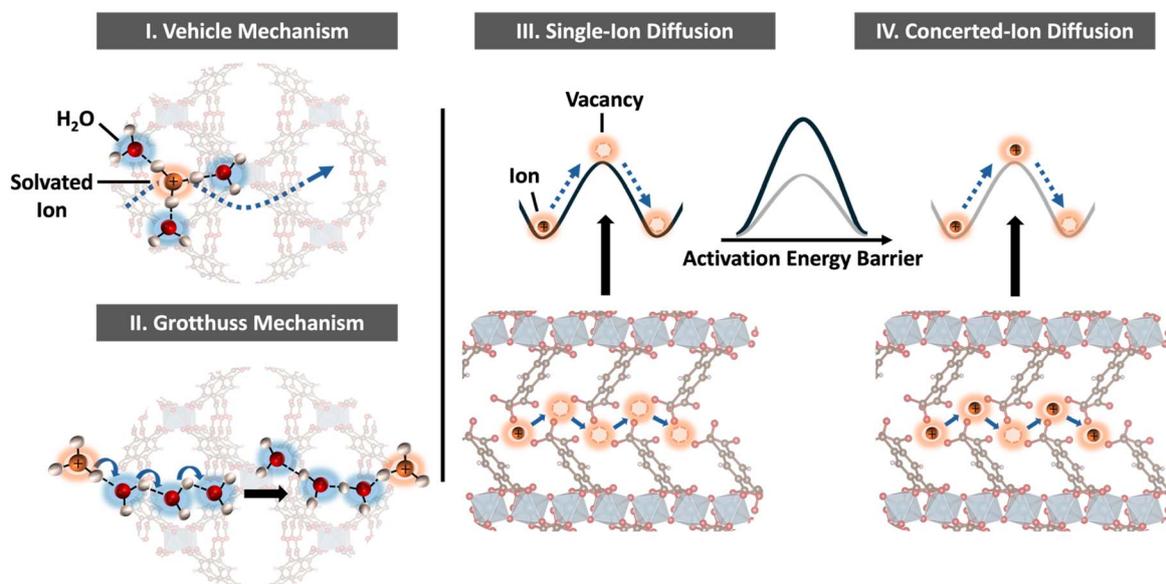

Fig. 2 Schematic representation of the four primary ion conduction mechanisms in porous or framework-based electrolytes. (I) Vehicle mechanism involves the migration of solvated ions through the material. (II) Grotthuss mechanism describes proton hopping facilitated by hydrogen-bond rearrangements, enabling rapid ion transport without the bulk motion of water molecules. (III) Single-ion diffusion proceeds *via* a vacancy-assisted hopping process, in which isolated ions overcome an activation energy barrier to move between coordination sites. (IV) Concerted-ion diffusion features cooperative hopping of multiple ions, which lowers the effective activation energy and enables enhanced conductivity, particularly in ordered frameworks or densely populated channels. Panels III and IV were adapted with permission from ref. 34.

This journal is © The Royal Society of Chemistry 2025

J. Mater. Chem. A, 2025, **13**, 33012–33033 | **33015**

(2D) MOF, Ti-dobdc (Fig. 3a), into which lithium halide salts (LiX, X = Cl, Br, I) were mechanically incorporated.[46] In their approach, Ti-dobdc and the lithium salts were ground together in a 1:1 molar ratio, followed by exposure to high humidity (95% RH), targeting the intercalation of LiX between the MOF layers. This mechanical insertion expanded the lattice and introduced ionic species without compromising the structural integrity of the framework. The resulting composites exhibited high total ionic conductivity ($>10^{-2}$ S cm^{-1}) between 30 and 40 °C. Notably, pulsed-field gradient (PFG) NMR revealed that this conductivity stemmed not only from Li$^+$ but also from substantial proton mobility, indicating mixed conduction. Interestingly, higher temperatures led to increased water uptake – a counterintuitive effect. Rather than promoting dehydration, elevated temperatures increased the framework's moisture content, a result attributed to the hygroscopic nature of the lithium salts, especially LiI. Higher water vapor pressure and weaker Li–X bond strength at elevated temperatures facilitated salt hydration, thereby enhancing the framework's affinity for moisture. As water molecules diffused into the structure, they formed hydrogen-bonded networks that supported proton conduction via the Grotthuss mechanism, evidenced by the low activation energies ($\sim$0.4 eV). This behavior is illustrated in Fig. 3, which shows the structure of Ti-dobdc along with the dependence of total ionic conductivity and activation energy on relative humidity. The data confirm that proton conduction becomes dominant under high humidity conditions, with activation energies dropping below 0.4 eV, consistent with a Grotthuss-type mechanism.

Even in MOFs where electronic conductivity is expected to dominate, proton interference can distort results. Wang et al. reported this in Cd$_2$(TTFTB), a 3D framework composed of Cd(II) and tetrathiafulvalene-tetrabenzoate ligands (TTFTB^{4-}).[47,48] This MOF is electrically conductive due to π–π interactions between the TTFTB linkers, which enable through-space electron transport. However, under humid conditions, the measured conductivity notably increased. Detailed analyses showed that water uptake introduced protonic conduction within the MOF, enhancing the measured conductivity. Spectroscopic analysis and conductivity measurements under varying partial pressures revealed that adsorbed water formed hydrogen-bonded networks along the TTFTB stacks, enabling proton hopping through the framework and significantly increasing the apparent conductivity (by one to two orders of magnitude relative to dry conditions).

Even aprotic vapors can obscure intrinsic ion transport behavior by introducing extrinsic conduction pathways. Yoshida et al. demonstrated this in MIL-101 (Fig. 4a) loaded with magnesium bis(trifluoromethanesulfonyl)imide (Mg(TFSI)$_2$) and exposed to acetonitrile (MeCN) vapors, reporting a record-high Mg^{2+} conductivity of 1.9×10^{-3} S cm^{-1} at room temperature.[49] As shown in Fig. 4, guest vapor exposure had a profound impact on conductivity. The enhancement was attributed to MeCN molecules forming solvation shells around Mg^{2+} ions, thereby reducing electrostatic drag and enabling coordinated ion migration. However, Yoshida et al. further noted that the transference number analysis revealed only 41% of the current originated from Mg^{2+}, with the remainder arising from protons and other solvated ions, underscoring the influence of the vapor environment on the observed conductivity. Similarly, Ulihin et al. found that MIL-101 impregnated with lithium perchlorate (LiClO$_4$) exhibited conductivity values typical of aqueous salt solutions ($\sim$10^{-3} S cm^{-1}) under 50% relative humidity, due to spontaneous water uptake.[50] This absorbed moisture formed a confined liquid phase within the pores, behaving as a proton-conducting electrolyte. Complete dehydration required
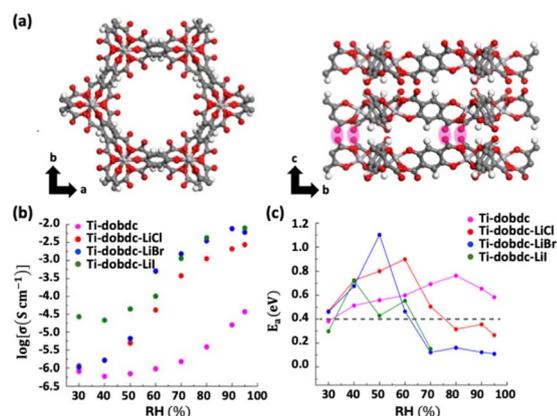

Fig. 3 (a) Structural model of the 2D-layered MOF Ti-dobdc, illustrating the hexagonal pore channels and highlighting in pink the non-coordinated carboxyl oxygen. (b) Ionic conductivity of Ti-dobdc and Ti-dobdc−LiX (X = Cl, Br, I) measured at 298 K under varying relative humidity (RH). (c) Corresponding activation energy values vs. RH. Adapted from ref. 46 with permission from Wiley-VCH, copyright 2023.
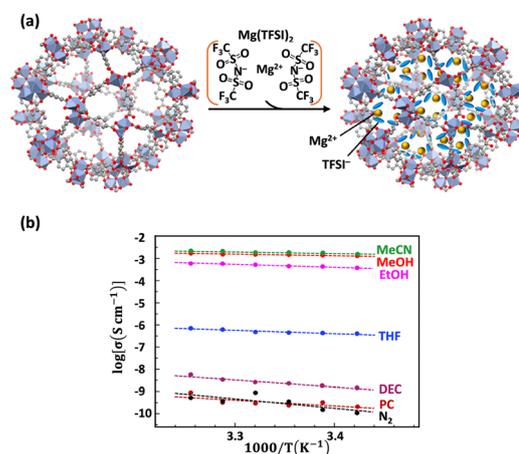

Fig. 4 (a) Structural illustration of MIL-101⊃{Mg(TFSI)$_2$}, showing the incorporation of Mg^{2+} and TFSI$^-$ within the framework pores. (b) Arrhenius plots of ionic conductivity for MIL-101⊃{Mg(TFSI)$_2$} under various anhydrous vapors. Exposure to MeCN, methanol (MeOH), and ethanol (EtOH) vapors significantly enhances conductivity ($>10^{-3}$ S cm^{-1}), whereas tetrahydrofuran (THF), diethyl carbonate (DEC), propylene carbonate (PC), and dry N$_2$ result in poor conductivity. Adapted from ref. 49 with permission from the American Chemical Society, copyright 2022.

33016 | J. Mater. Chem. A, 2025, 13, 33012–33033

This journal is © The Royal Society of Chemistry 2025

prolonged vacuum heating at 180 °C, confirming the persistent nature of this extrinsic contribution.

Beyond vapor-mediated effects, ambient exposure can destabilize composite MOF electrolytes, complicating conductivity interpretation. Nozari *et al.* studied a Na-conducting IL@ZIF-8 composite (IL: ionic liquid, ZIF: zeolitic imidazolate frameworks) that initially exhibits an ionic conductivity of $\sim 2 \times 10^{-4}$ S cm^{-1} at 25 °C.[51] When stored in $\approx 45\%$ RH air, the crystalline sample's conductivity falls by $\approx 8\%$ after 2 days and $\approx 30\%$ after 20 days, with activation energy rising from 0.26 eV to 0.38–0.40 eV. To address this, the composite was ball-milled for 30 minutes to yield a partially amorphous material (am-S-IL@ZIF-8). Although its initial conductivity was lower ($\sigma_0 = 2.97 \times 10^{-5}$ S cm^{-1}), the amorphous sample retained approximately 85% of its conductivity over 20 days, in contrast to a decline of over 30% in the crystalline analogue. The authors attribute this enhanced retention to reduced framework–guest interactions in the disordered network, which better preserves Na$^+$ pathways. However, because neither ionic liquid leaching nor water-uptake isotherms are directly measured, the assertion that amorphization alone confers the improved air stability remains inferential and would benefit from targeted sorption or humidity control studies.

2.3 Distinguishing intrinsic *vs.* extrinsic ionic conductivity

A central insight from the studies discussed in Section 2.2 is the importance of distinguishing intrinsic from extrinsic ionic conduction in MOF-based electrolytes. Intrinsic conduction arises when the MOF structure itself facilitates ion transport, either through functionalization with fixed ionic groups, such as sulfonate, carboxylate, or phosphonate moieties, or *via* framework-embedded pathways that enable ion hopping without the aid of external solvents. For instance, in MIL-53(Al)@LiCoD, Li$^+$ conduction occurs intrinsically through a hopping mechanism facilitated by the rotation of carborane anions and the inherent flexibility of the framework.[45] Similarly, Mg(TFSI)$_2$@MIL-101 exhibits modest conductivity, attributed to Mg^{2+} diffusion between TFSI$^-$ coordinated within the MIL-101 pore.[49] Intrinsic proton conductors are also well documented, particularly in MOFs containing coordinated water molecules or acidic groups. These systems can enable Grotthuss-type proton hopping through a continuous hydrogen-bond network, independent of external humidity. For example, MOFs loaded with mobile acids like CSH·SO$_4$ (cysteine hydrogen sulfate) or H$_2$SO$_4$ (sulfuric acid) exhibit high intrinsic proton conductivity when the acid species are chemically integrated into the framework.[50] In all these cases, the materials qualify as true solid-state conductors in their dry or chemically bound state.

On the other hand, extrinsic conduction emerges when external vapors or liquids infiltrate the MOF, creating liquid-like environments within the pores. Water is the most prevalent contributor, as many MOFs are hydrophilic and readily adsorb moisture under ambient conditions.[45,46,50] Once adsorbed, water can dissociate to form H$_3$O$^+$ or OH$^-$ in the presence of polar sites or promote ion solvation and mobility. For example, in the previously discussed LiClO$_4$-loaded MIL-101, moisture uptake led to the formation of a liquid much like brine in the pores.[50] Under these conditions, the measured conductivity was dominated by a vehicle-type mechanism, in which solvated ions migrate through a confined liquid phase, rather than by solid-state hopping. This phenomenon is best described as quasi-solid-state conduction, a hybrid regime that blurs the line between a rigid solid electrolyte and a bulk liquid system. Quasi-solid-state conduction typically results from these extrinsic effects, where guest solvents, whether introduced intentionally or through ambient exposure, form fluid-like ion pathways within the MOF. These systems often display low activation energies, comparable to those of liquid or gel electrolytes, which can artificially inflate the apparent performance of the material.[44] For instance, Hou *et al.* demonstrated that even MOFs with built-in ion hopping groups can exhibit enhanced conductivity when solvent molecules like propylene carbonate transiently assist ion migration between binding sites.[44] In this study, the propylene carbonate-filled MOF was investigated as part of a mechanistic analysis to elucidate ion transport pathways, rather than as a direct performance comparison to the unfilled material.

To reliably distinguish intrinsic from extrinsic conduction pathways, it is essential to apply a combination of complementary techniques, such as environmentally controlled impedance measurements, transference number analysis, and *in situ* NMR or vibrational spectroscopies – ideally supported by molecular simulations. Only under strictly anhydrous conditions can the actual contribution of the MOF to ionic transport be reliably assessed. Without such control, the system may operate in a quasi-solid-state regime, where conductivity arises from confined liquid phases rather than from genuine solid-state ion hopping. While these hybrid transport modes can exhibit high ionic conductivity, they often lack the long-term stability and consistent performance required for solid-state battery applications – attributes essential for ensuring reliable and predictable operation over time.

From a mechanistic standpoint, ion conduction in MOFs can shift from being governed purely by hopping between framework-coordinated sites to involving liquid-like mechanisms, such as Grotthuss-type proton hopping or vehicle conduction by solvated ions. While intrinsic proton conductors rely on built-in hydrogen-bond networks to enable such transport, extrinsic conduction emerges when water infiltrates the pores and bridges donor and acceptor sites. A key indicator of such behavior is low activation energy (often 0.1–0.4 eV in MOFs), comparable to hydrated polymer or liquid electrolytes, and significantly lower than the activation energies associated with structural ion-hopping in a dry solid.[44,51]

Disentangling these effects requires careful experimental controls. One widely used approach is to measure conductivity under rigorously anhydrous conditions, such as inside a glovebox, to eliminate or reduce the effect of protonic conduction to a negligible level. Another diagnostic is drying reversibility; intrinsic conductivity should remain the same after drying, whereas extrinsic contributions typically diminish or disappear once the material is dried. This was demonstrated in Cd$_2$(-TTFTB), where conductivity sharply decreased when switching

This journal is © The Royal Society of Chemistry 2025

J. Mater. Chem. A, 2025, **13**, 33012–33033 | **33017**

from a humid to a dry atmosphere, confirming the extrinsic nature of the proton conduction.[48] The work by Yoshida *et al.* reinforces this point, as the Mg^{2+} transference number of 0.41 further illustrates how a significant portion of the current in "multivalent-conducting" MOFs may originate from protonic species.[49] Therefore, to avoid misinterpretation, rigorous control over humidity and residual solvents, coupled with techniques such as transference number measurements, *in situ* spectroscopy, and glovebox-based EIS, should be standardized when evaluating MOF-based electrolytes for targeted ion transport. Only by systematically excluding extrinsic proton conduction can reported values be considered representative of true ionic conductivity.[51]

3 Interfacial contact

Interfacial contact between MOF-based electrolytes and electrodes is a defining factor in the performance of solid-state batteries. It governs ion transport, electrochemical stability, and mechanical integrity.[52,53] Unlike liquid electrolytes that form self-healing, conformal interfaces during cycling, solid electrolytes often form rigid, heterogeneous junctions with electrodes.[54,55] In the case of MOF-based electrolytes, their rigid and microcrystalline nature frequently results in poor interfacial contact with electrodes, producing high interfacial resistance that impedes lithium-ion transfer and reduces overall battery performance. These interfaces are complex, involving intertwined physical, chemical, and electrochemical interactions that collectively impact device efficiency, stability, and safety.[53,54]

3.1 Physical contact and structural heterogeneity

The rigid morphology, microcrystalline texture, and poor deformability of MOFs often result in incomplete physical contact, leading to interfacial voids that hinder lithium-ion transport and increase resistance.[53–55] This section explores two key aspects of this challenge: (1) Causes of limited interfacial contact, and (2) Strategies to mitigate physical contact. Together, these subsections highlight how interfacial engineering can enhance contact quality, reduce resistance, and improve overall battery performance.

3.1.1 Causes of limited interfacial contact. MOFs often exhibit inherently poor physical contact with solid electrodes, which leads to high interfacial resistance that impedes lithium-ion transfer and ultimately reduces overall battery performance. This limitation arises from their typical synthesis as microcrystalline powders with irregular particle sizes and rigid angular morphologies. Their contact with electrodes is primarily physical, and the mismatch between stiff MOF particles and uneven electrode surfaces further limits adhesion. Grain boundaries, voids, and surface roughness at the MOF–electrode interface form localized high-resistance regions, often referred to as "dead zones", which impede ion transport (Fig. 5).[55,56] This issue is further compounded by the intrinsic rigidity and brittle nature of most MOFs, which prevents them from conforming to softer, more flexible materials such as
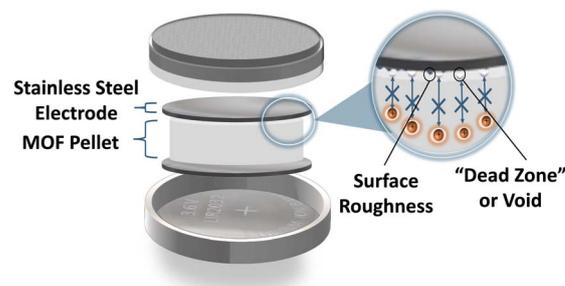

Fig. 5 Schematic of the MOF-based solid electrolyte–electrode interface highlighting interfacial limitations. Rigid MOF pellets, typically formed from microcrystalline powders, exhibit surface roughness and morphological mismatch with the electrode, leading to poor physical contact. The resulting voids and grain boundary gaps form "dead zones" that impede ion transport and contribute to interfacial resistance.

polymer matrices or organic binders, resulting in interfacial gaps.[20,57–63] Particle size also plays a critical role: smaller MOF particles provide higher external surface area and improved packing density, promoting better contact with electrode surfaces.[63,64] In contrast, larger crystallites, particularly on rough surfaces, pack inefficiently, creating voids both within the MOF layer and at the MOF–electrode interface.[57,64] Research on hexagonal Ni-MOFs by Ghamari *et al.* showed that reduced particle size improved electrode durability and performance, likely due to improved packing density and reduced void formation.[64] The surface roughness of MOFs and electrodes critically influences interfacial resistance and the charge transfer efficiency. A significant mismatch in surface roughness between the two materials can drastically reduce the effective contact area, thereby impeding ion transport.[65–67] A common approach for evaluating the ionic conductivity of MOFs involves compressing the material into pellets, which are then placed between stainless steel blocking electrodes.[68] Felice *et al.* found that increasing the surface rugosity of stainless steel electrodes led to a reduction in exchange current, suggesting that rougher electrode surfaces hinder efficient charge transfer due to poor interfacial matching.[69] This mismatch is further highlighted by roughness measurements: MIL-53(Al) pellets have a surface roughness of approximately 100 nm,[70] while stainless steel plates typically range from 0.3 to 1.0 μm.[71] This illustrates the potential scale of this mismatch and its potential to introduce significant interfacial contact resistance.

3.1.2 Strategies to mitigate physical contact. Addressing the intrinsic challenges of physical contact and structural heterogeneity at the electrode and MOF electrolyte interface is critical to enhancing solid-state battery performance. These challenges, stemming from mismatches in mechanical properties, crystalline morphologies, and surface roughness, significantly impact ion transport efficiency and interfacial resistance. Various strategies have emerged to overcome these limitations, including doping MOFs with liquid electrolytes, applying external pressure, blending MOFs with polymer fillers, and adopting slurry casting or spray-coating techniques. Each

33018 | *J. Mater. Chem. A*, 2025, **13**, 33012–33033

This journal is © The Royal Society of Chemistry 2025

approach targets improved interfacial stability and ion transport through distinct mechanisms.

Among the most studied approaches is doping MOFs with liquid electrolytes. By confining the liquid phase within the MOF's porous architecture, this approach can significantly improve ion transport pathways. Farina *et al.* demonstrated this in Mg-MOF-74 soaked with a mixture of LiClO$_4$ and propylene carbonate (PC), referred to as LiClO$_4$–PC@MgMOF-74, which achieved a conductivity of 1.4×10^{-4} S cm^{-1} at 20 °C.[72] The authors attributed this enhancement to three key factors: (1) nanoconfinement effects that stabilize the electrolyte within the pores, (2) strong host–guest interactions between the MOF framework and the liquid electrolyte, and (3) preservation of the MOF's structural integrity, which supports uninterrupted ion migration.

Beyond electrolyte incorporation, pressure-assisted methods can significantly enhance interfacial contact and, in some cases, activate novel ion transport pathways. Ortiz *et al.* showed that applying pressure to ZAG-6 induces a linker coiling mechanism in its hexanediphosphonate chain, which reduces interatomic distances and enables pressure-driven Grotthuss-like proton hopping conduction.[73] As shown in Fig. 6, O–H bond distances in H$_2$O and PO$_3$H shift abruptly above 3 GPa, signaling a pressure-driven proton transfer, a rare instance of mechanically induced conduction in MOFs. Similarly, Yoshida *et al.* found that the ionic conductivity of MIL-101 loaded with Mg(TFSI)$_2$ drastically increases with higher MeCN partial pressure, particularly at low pressures.[49] Conductivity reached superionic levels above 10^{-3} S cm^{-1} due to efficient Mg^{2+} migration facilitated by adsorbed MeCN molecules. For Li$^+$ conductors, applying pressure is also common practice to boost conductivity, though care must be taken to avoid damaging the MOF's rigid structure – a topic discussed further in Section 3.3.[68]

Another practical strategy involves fabricating freestanding composite membranes by integrating MOFs with flexible polymer. These hybrid materials enhance mechanical compliance, improve electrode adhesion, and suppress interfacial resistance while preserving the ion-conductive functionality of MOFs. For example, a composite membrane was fabricated *via in situ*
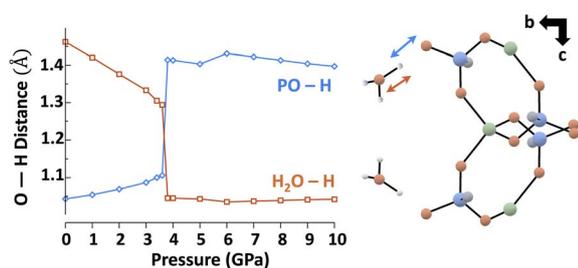
coordination of ZIF-67 with lithium alginate (LA) and polyacrylamide (PAM), forming a robust three-dimensional (3D) polymer–MOF network.[74] This material significantly enhanced mechanical strength, facilitated uniform lithium-ion deposition, and maintained both high ionic conductivity and excellent electrochemical stability. Similarly, Cheng *et al.* developed a freestanding electrolyte based on UiO-66, poly(vinylidene fluoride-*co*-hexafluoropropylene) (PVDF-HFP), and an ionic liquid (IL) composed of lithium bis(trifluoromethanesulfonyl) imide (LiTFSI) and 1-ethyl-3-methylimidazolium bis(trifluoromethylsulfonyl)imide ([EMIM][TFSI]).[75] The resulting membrane combined the high porosity of the MOF with the flexibility of the polymer matrix, achieving a high ionic conductivity of 5.55×10^{-4} S cm^{-1} and a Li$^+$ transference number of 0.52, along with excellent mechanical strength (6.63 MPa) and interfacial stability. These examples highlight how MOF–polymer composites can effectively address challenges related to interfacial contact and mechanical durability in solid-state electrolyte systems.

Surface-deposition methods such as slurry casting and spray-coating offer another practical pathway to enhance MOF–electrode adhesion. These techniques are particularly effective at anchoring MOF particles onto electrode surfaces, thereby enabling intimate physical contact and reducing interfacial resistance.[62,76] In this context, Lin *et al.* developed a composite by dispersing ZIF-62 particles into a polyimide (6FDA-DAM) matrix, followed by vitrification of the MOF phase.[62] Upon thermal treatment, the ZIF-62 crystals transformed into an amorphous glass that filled interfacial voids and formed Zn–O and Zn–F bonds with the polymer, reducing void volume by 79% and significantly improving interfacial contact (Fig. 7).

Similarly, combining MOFs with polymeric binders like polyvinylidene fluoride (PVDF) *via* slurry casting can also produce conformal composite coatings that bridge interfacial gaps and facilitate continuous ion conduction. For instance, Fischer *et al.* prepared a slurry of Al-Td-MOF-1 and PVDF, which they cast onto aluminium foil, achieving an ionic conductivity of 5.7×10^{-5} S cm^{-1}.[77] However, a common challenge with this approach is the difficulty in uniform and well-distributed MOF coatings due to the bulky and often irregular morphology of MOF crystals.[78] Despite this limitation, slurry casting and spray-

Fig. 6 (Left) Pressure dependence of O–H bond distances in R–PO$_3$H (blue) and H$_2$O (orange) in ZAG framework. Above 3 GPa, the abrupt crossover in distances indicates a proton transfer from H$_2$O to the phosphonate group, consistent with the onset of Grotthuss-type proton conduction. (Right) Structural illustration of the local environment showing the water molecule, phosphonate group, and the two relevant O–H distances indicated by arrows. Adapted from ref. 73 with permission from the American Chemical Society, copyright 2014.
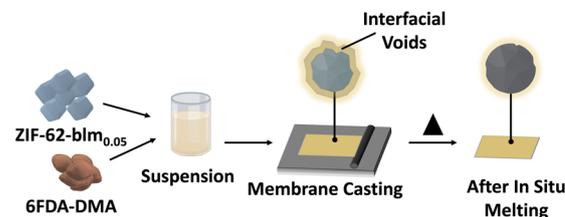

Fig. 7 Schematic of the fabrication process for a mixed-matrix membrane using ZIF-62 and polyimide (6FDA-DAM). Crystalline ZIF-62 is dispersed into the polymer, cast into a membrane, and subjected to thermal treatment to induce *in situ* vitrification. Upon melting, the ZIF-62 forms an amorphous glass (agZIF-62) that fills interfacial voids and improves contact with the polymer matrix, enhancing mechanical integrity and interfacial bonding. Adapted from ref. 62.

This journal is © The Royal Society of Chemistry 2025

J. Mater. Chem. A, 2025, **13**, 33012–33033 | **33019**

coating remain essential fabrication tools for balancing interfacial engineering and scalable manufacturing, key considerations for integrating MOF-based electrolytes into practical devices.

3.2 Chemical reactivity at the interface during cycling

Beyond structural compatibility, the long-term performance of MOF-based electrolytes is critically influenced by their chemical reactivity at the electrode interface. During electrochemical cycling, MOFs are subjected to highly reducing or oxidizing conditions. Their chemically accessible pores, potentially reactive functional groups, and, in some cases, open metal coordination sites can undergo decomposition or side reactions, leading to parasitic byproducts and the formation of unstable interfaces.[56,79,80] These degradation processes produce decomposition products, such as inorganic salts or polymeric species. The accumulation of these products forms electronically insulating layers at the interface, increasing charge-transfer resistance, impeding ion migration, and accelerating capacity fade. Addressing this chemical instability is therefore essential for maintaining long-term battery performance. This section explores interfacial chemistry challenges, organized into four key categories. First, Space-charge effects, where electrochemical potential mismatches at the electrode–electrolyte interface cause ionic redistribution and the formation of resistive interfaces. Second, Wetting behaviour, highlighting how poor interfacial contact under dynamic cycling conditions leads to uneven current distribution and dendrite formation. Third, MOF-based composites and interfacial distribution focuses on how the spatial arrangement of MOFs within polymer matrices affects electrochemical stability and ion transport. Finally, Strategies to mitigate chemical reactivity at the interface under dynamic conditions discusses approaches such as linker functionalization, controlled MOF dispersion, and targeted ion coordination, all aimed at reducing interfacial degradation and enhancing long-term stability. Collectively, these topics provide a comprehensive view of MOFs' chemical limitations in battery environments and the strategies to address them.

3.2.1 Space charge effects. At MOF-based electrolyte–electrode interfaces, differences in lithium chemical potential can induce the formation of space-charge layers – interfacial regions of ionic redistribution, analogous to those observed in ceramic electrolytes.[56,81,82] These layers are characterized by local charge accumulation or depletion and have been shown to impede Li^+ transfer, increasing interfacial resistance.[82] Cheng *et al.* demonstrated that such a space-charge layer at the interface between the solid electrolyte $Li_{1.5}Al_{0.5}Ge_{1.5}(PO_3)_4$ (LAGP) and the cathode material $(Li_xV_2O_5)$ resulted in a substantial increase in the activation energy for Li^+ diffusion and led to nearly a fourfold rise in interfacial resistance. Although MOF-specific studies on space-charge phenomena remain limited, similar effects are anticipated.[56,83–86]

Lu *et al.* highlighted that Li^+ transport in MOF electrolytes is sensitive to interfacial properties, indicating that even a framework whose bulk structure has been "optimized" for rapid ion hopping can develop space-charge layers at its boundaries.[56] As

illustrated in Fig. 8, these effects can manifest as charge-separated regions at the cathode–electrolyte interface, giving rise to local electric field gradients. Anionic MOFs are often employed to immobilize counterions and improve the Li^+ transference number, reducing bulk ion polarization.[83] However, at poorly integrated or chemically mismatched interfaces, ion accumulation and field-induced polarization can still occur – a topic that remains underexplored for MOFs.

The oxidative stability of MOFs is another critical consideration, especially when paired with high-voltage cathodes. Although some MOFs possess relatively wide electrochemical stability windows, many undergo oxidative decomposition.[87,88] This degradation leads to the formation of cathode–electrolyte interfaces (CEIs) composed of electronically insulating species, which hinder lithium-ion transport, increase interfacial impedance, and degrade battery performance and cycling life.[89] The formation of such decomposition layers has also been shown to compromise both the chemical and mechanical integrity of the electrolyte.

Similarly, under reducing conditions at the lithium metal anode, MOFs may undergo chemical degradation by reducing metal nodes or cleavage of organic linkers, leading to interfacial decomposition layers.[89] Although direct *operando* evidence of such degradation remains limited, Mu *et al.* have emphasized the intrinsic chemical vulnerabilities of MOFs and the pressing need for systematic *in situ* studies to elucidate degradation mechanisms.[90]

3.2.2 Wetting behavior and contact quality. Wetting behavior becomes particularly critical under cycling, where maintaining intimate and stable contact between the MOF-based electrolyte and the electrode is essential for reliable
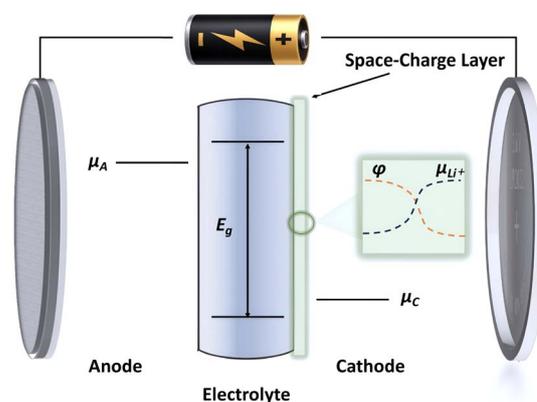
Fig. 8 Schematic of a MOF-based solid electrolyte cell, illustrating the formation of a space-charge layer at the electrolyte–cathode interface. Differences in lithium chemical potential (μ_A and μ_C) between the anode and cathode drive the redistribution of Li^+ ions, resulting in the formation of a charged interfacial region. The MOF electrolyte is represented as an electronically insulating medium with a sufficient bandgap (E_g), and the shaded regions at the interfaces indicate space-charge formation. The inset shows the spatial variation of the electrochemical potential of Li^+ (μ_{Li^+}) and the electrostatic potential (φ) near the cathode interface. These local field gradients hinder Li^+ migration and contribute to interfacial resistance, particularly in MOFs with imperfect contact or mismatched chemical environments.

33020 | *J. Mater. Chem. A*, 2025, **13**, 33012–33033

This journal is © The Royal Society of Chemistry 2025

performance. Wetting refers to the electrolyte's ability to form both continuous and conformal contact with the electrode surface during operation.[80] Incomplete wetting can lead to the formation of microscale interfacial voids that trap gases or impurities, promoting parasitic side reactions and increasing interfacial resistance. These issues are particularly problematic during lithium plating and stripping, where poor contact results in non-uniform current distribution.[91,92] This, in turn, drives localized lithium deposition, the formation of unstable solid electrolyte interfaces (SEI), and ultimately dendrite growth; factors that compromise both performance and safety. Lee *et al.* demonstrated that for lithium lanthanum zirconate (LLZO)-based solid-state batteries, where insufficient wetting at the Li–electrolyte interface led to increased interfacial resistance, necessitating high-temperature sintering or pressure-assisted densification to achieve adequate contact.[93,94]

A compelling example of how MOF design can enhance wettability is demonstrated by Wang *et al.*, who developed a solid-like composite electrolyte by impregnating a MOF with a lithium-containing ionic liquid (Li-IL@MOF).[95] The confined ionic liquid formed nanoconformal interfacial layers, termed "nanowetted interfaces", at the electrode–electrolyte boundary, significantly improving interfacial contact and reducing void formation (Fig. 9). This design enabled low and stable interfacial resistance, uniform Li deposition, and improved cycling stability, even under high current densities. Scanning electron microscopy (SEM) and EIS analyses confirmed that these nanowetted interfaces played a key role in suppressing interfacial degradation.

3.2.3 MOF-based composites and interfacial distribution.

While polymer-based composites offer a promising route to enhance the processability and interfacial integration of MOF-based electrolytes, their long-term performance critically depends on the spatial organization of the MOFs within the polymer matrix. In composite polymer electrolytes (CPEs), the mere inclusion of MOFs is not always sufficient – microstructural uniformity and connectivity play a crucial role in their

performance. Poor dispersion or agglomeration of MOF particles can lead to discontinuous conductive pathways, phase separation, and mechanical inhomogeneities, all of which contribute to uneven Li⁺ flux, localized current density hotspots, and ultimately, the growth of lithium dendrites.

Li *et al.* demonstrated that such microstructural irregularities in MOF-based composite electrolytes promote nonuniform lithium deposition and dendrite formation, ultimately compromising conductivity and cycling stability.[78,91] Achieving uniform dispersion, strong matrix interactions, and continuous percolation pathways is essential to avoid localized electrochemical degradation.[91] This is illustrated in Fig. 10, comparing a randomly dispersed MOF–polymer blend to a structured 3D architecture, highlighting how continuous Li⁺ pathways improve transport and suppress interfacial resistance.

3.2.4 Strategies to mitigate chemical reactivity at the interface under dynamic conditions.

Despite their promise, MOF-based electrolytes often suffer chemical degradation at the electrode interface during repeated charge–discharge cycles. Side reactions between reactive metal nodes or functional linkers and highly reducing or oxidizing electrode surfaces generate resistive interfaces and space-charge layers, raising interfacial impedance and undermining performance and safety. This section explores emerging strategies to overcome these interfacial challenges, focusing on methods that improve chemical robustness and interfacial stability during repeated charge–discharge cycles. Key approaches include chemical modification of MOF linkers, enhancing MOF dispersion within polymers, and using MOF metal sites to anchor reactive anions. These techniques represent a growing toolbox for stabilizing electrode–MOF electrolyte interfaces and pushing MOFs closer to practical solid-state battery applications.

An effective approach involves modifying the MOF's organic linkers with electron-withdrawing or redox-inert groups. By reducing the linker's susceptibility to redox reactions at the interface, these functionalizations help maintain structural integrity and promote a stable solid–electrolyte interface. For example, He *et al.* introduced fluorine atoms into UiO-66(Zr), yielding UiO-66-F$_4$, and embedded it within a PVDF-HFP matrix.[96] The electronegative F-atoms enhanced LiTFSI dissociation, raising the ionic conductivity to 4.37×10^{-4} S cm^{-1}, and stretched the electrochemical stability window to 4.9 V.
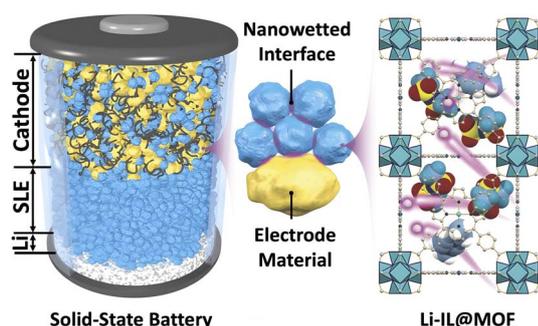

Fig. 9 Illustration of a Li-IL@MOF solid-like electrolyte showing multiscale interface structure. The left side shows the cross-sectional cell layout with nanowetted interfaces between the MOF–ionic liquid composite and electrodes. Zoomed-in interface in the center shows the nanowetted interface. The atomistic view on the left shows the randomly confined [EMIM]⁺, [TFSI]⁻, and Li⁺ within MOF pores. Adapted from ref. 95 with permission from Wiley-VCH, copyright 2018.
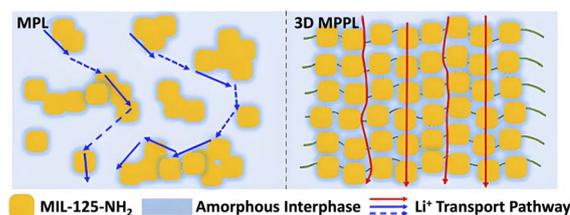
Fig. 10 Visual comparison of Li⁺ transport in a random MOF–polymer blend (MPL, left) *versus* a well-aligned 3D MOF–polymer percolated layer (3D MPPL, right). Random distribution leads to discontinuous ionic pathways and increased resistance, while structured 3D architectures enable efficient, continuous Li⁺ conduction. Adapted from ref. 91 with permission from AAAS, copyright 2023.

This journal is © The Royal Society of Chemistry 2025

J. Mater. Chem. A, 2025, **13**, 33012–33033 | **33021**

More importantly, the resulting SEI suppressed dendrite growth, enabling consistent cycling over 300 cycles without capacity loss.

Achieving uniform dispersion of MOF particles in polymer hosts is equally critical, as agglomeration creates localized transport barriers, uneven current distribution, and nucleation sites for dendrites. *In situ* polymerization, where monomers polymerize around dispersed MOF particles, has proven particularly effective. A recent study demonstrated that the incorporation of MOF-808 into a PEO matrix *via* this method produced a composite membrane with enhanced ionic conductivity and stable lithium plating behaviour.[97] Alternatively, surface functionalization of MOFs can promote compatibility with casting solutions: coating UiO-66 particles with polyimide oligomers leverages "like-dissolves-like" interactions to maintain colloidal stability, facilitating large-area PIM-1 membranes with uniform MOF integration.[98] This compatibility is visually demonstrated in Fig. 11, where the dispersibility of polyUiO-66(4 : 1) and pristine UiO-66 is compared across multiple solvents. This led to stable colloidal dispersions and uniform integration into large-area PIM-1 membranes, suggesting a promising route to scalable MOF–polymer composites. Gao *et al.* used coaxial electrospinning to embed ZIF-8 nanoparticles uniformly within PAN nanofibers, forming a flexible composite membrane with high ionic conductivity $(1.29 \times 10^{-3}$ S cm$^{-1})$, a Li$^+$ transference number of 0.79, and excellent interfacial contact.[99] Compared to conventionally mixed membranes, the electrospun structure prevented MOF aggregation and ensured smooth lithium deposition.

Another strategy includes leveraging the coordination properties of open metal sites in MOFs to selectively anchor mobile anions and suppress parasitic interfacial reactions. For example, Tian *et al.* incorporated a 3D interconnected Cu-MOF onto PAN nanofibers within a PEO-based solid-state electrolyte.[100] The Cu-MOF's open metal sites strongly anchored TFSI$^-$ anions and competed with Na$^+$ and PEO for coordination. This competitive binding promoted greater Na$^+$ dissociation, reduced Na$^+$–O interactions, and led to the formation of SEIs and CEIs rich in NaF and Na$_3$N, materials known for their ionic conductivity and mechanical robustness. As a result, the composite electrolyte demonstrated enhanced Na$^+$ mobility, excellent interfacial stability with over 1000 hours of cycling, and superior full-cell performance over 2000 cycles. Collectively, these strategies, from linker functionalization to uniform MOF dispersion and anion anchoring, directly target the suppression of decomposition product formation, thereby mitigating resistance buildup and preserving long-term electrochemical performance.

3.3 Mechanical stress

Although most research on MOF-based electrolytes emphasizes ionic conductivity and interfacial chemistry, their intrinsic brittleness under cycling-induced stress can equally undermine long-term reliability. Solid-state batteries impose mechanical challenges, from electrode volume changes and thermal fluctuations to external pressure, that crystalline MOF architectures must withstand. This section is organized into three parts: (1) Inherent mechanical properties of MOFs, introducing fundamental metrics and discussing how frameworks respond to stress and strain. (2) Mechanical effects based on the crystalline nature of MOFs, examining how metal–linker connectivity, linker length, and functional groups govern resilience and brittleness; and (3) Strategies to mitigate mechanical stress in MOF-based electrolytes, highlighting emerging MOF–polymer composites that impart flexibility, durability, and adaptability during operation. Together, these parts offer a unified view of how mechanical properties shape the design of robust MOF electrolytes for practical battery applications.

3.3.1 Inherent mechanical properties of MOFs. The mechanical properties of MOFs are crucial in determining their applicability as electrolytes in solid-state batteries. To understand MOF mechanics, we begin with fundamental concepts, specifically through essential equations governing stress and strain relationships.[101]

Stress (σ) typically in Pa is defined as the applied force (F) in N per unit area (A) in m^2:

$$\sigma = \frac{F}{A} \quad (6)$$

The response to stress is quantified by strain (ε), which is dimensionless, representing the relative deformation:

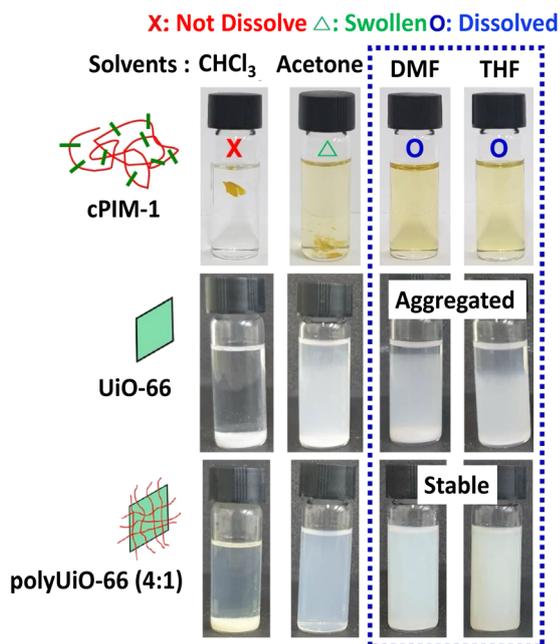$$\varepsilon = \frac{\Delta L}{L_0} \quad (7)$$

Fig. 11 Comparison of dispersion behavior for pristine UiO-66, polyUiO-66(4 : 1), and cPIM-1 in various solvents (CHCl$_3$, acetone, DMF, and THF). Functionalization with cPIM-1 improves compatibility in polar aprotic solvents (DMF and THF), resulting in stable colloidal dispersions of polyUiO-66(4 : 1), while unmodified UiO-66 shows aggregation and sedimentation. Stable dispersions facilitate uniform MOF integration into polymer matrices. Adapted from ref. 98 with permission, copyright 2023.

33022 | *J. Mater. Chem. A*, 2025, **13**, 33012–33033

This journal is © The Royal Society of Chemistry 2025

Here, ΔL is the change in length, in units m, and L_0 is the original length of the material.

In the elastic regime, stress and strain are linearly related according to Hooke's law:

$$\sigma = E\varepsilon \tag{8}$$

where E is Young's modulus, a measure of the material's stiffness in Pa, given by:

$$E = \frac{\sigma}{\varepsilon} \tag{9}$$

The mechanical response of MOFs also includes transverse deformation quantified by Poisson's ratio (ν), typically dimensionless, defined as the ratio of transverse strain to longitudinal strain:

$$\nu = -\frac{\varepsilon_{\text{transverse}}}{\varepsilon_{\text{longituudal}}} \tag{10}$$

The material's resistance to shear deformation is captured by the shear modulus (G) in Pa, defined as the ratio of shear stress (τ) Pa to shear strain (γ):

$$G = \frac{\tau}{\gamma} \tag{11}$$

Additionally, the volumetric stiffness under uniform hydrostatic pressure (P) in Pa is characterized by the bulk modulus (K) also in Pa:

$$K = -\frac{P}{\Delta V / V_0} \tag{12}$$

MOFs generally exhibit mechanical brittleness due to their rigid coordination bonds and limited capacity for plastic deformation within their crystalline lattice. This inherent brittleness poses significant challenges when MOFs are subjected to mechanical stresses by external pressures, thermal fluctuations, or volume changes during operational cycles. Table 1 summarizes experimental and computational values of E, K, and G for selected MOFs reported in the literature, which will be discussed in the following sections.

3.3.2 Mechanical effects based on the crystalline nature of MOFs.
While significant research on MOF-based electrolytes has focused on maximizing ionic conductivity, their mechanical integrity under cycling-induced stress is just as crucial for long-term performance. The inherently brittle nature of many MOFs struggles to accommodate the repeated expansion and contraction of battery electrodes, resulting in crack formation, loss of interfacial contact, and ultimately degraded ionic pathways.[23,121,122] This section explores how the mechanical properties of MOFs, governed by their metal nodes, linker lengths, connectivity, and functionalization, affect their structural resilience.

At a fundamental level, a MOF's mechanical behavior is captured by metrics such as Young's modulus to quantify its stiffness and resistance to volume change. Rigid frameworks like UiO-66(Hf) (30–60 GPa) and UiO-66(Zr) (22–45 GPa) maintain dimensional stability under static loads, yet they can become liabilities under cycling when localized mechanical stress accumulates at the electrode–MOF interface (Table 1).[102] In contrast, softer structures, MOF-5 or HKUST-1, offer greater flexibility but sacrifice the support needed to preserve continuous ion-conducting channels. Striking the right balance between stiffness and toughness is key to preventing fracture without undermining overall structural integrity.[123]

A key design parameter for tuning MOF mechanical properties is the length of the organic linker. Longer linkers generally introduce greater flexibility into the framework, allowing the structure to accommodate strain. However, this flexibility often comes at the expense of reduced mechanical strength.[115,116,124] Banlusan et al.'s used density functional theory (DFT) to determine the mechanical properties of various isoreticular MOFs such as IRMOF-1, IRMOF-10, and IRMOF-16, as well as UiO-66, UiO-67, and MOF-801.[115] Their work showed that Young's modulus decreased as the linker length increased, imparting additional framework flexibility at the cost of reduced load-bearing capacity. Similarly, Krause et al. examined a series of DUT-49 derivatives (DUT-48, 46, 49, 50, and 151) and found that longer linkers invariably lower the framework's stress tolerance.[116] This trade-off between crystallinity and flexibility underscores the importance of carefully choosing linkers or using hierarchical structuring to prevent fractures and ensure long-term durability in solid-state batteries.

Beyond linker length, the connectivity between the metal node and organic linker also plays a pivotal role in determining a MOF's mechanical behavior. This connectivity governs how mechanical stress is distributed throughout the framework – higher connectivity yields stiffer and more compression-resistant frameworks. For instance, Celeste et al. found that MIL-100(Cr) had superior stability under compression, with a bulk modulus almost ten times larger than MIL-101(Cr).[118] The superior stability of MIL-100(Cr) stems from its tritopic linkers and Cr nodes, which form more highly interconnected networks than the ditopic linkers in MIL-101(Cr). The role of metal-node identity was further explored by Rogge et al., who studied a series of UiO-66 frameworks incorporating Zr, Ce, Hf, and mixed-metal compositions (3Zr:3Ce and 3Zr:3Hf).[125] Their results showed that Zr-based UiO-66 had the highest mechanical resilience, retaining crystallinity under pressures up to 1400 MPa. This was followed by Hf (620 MPa), the mixed Zr–Hf variant (210 MPa), and Ce-based frameworks (100 MPa). Fig. 12 illustrates this trend, presenting pressure-dependent PXRD patterns for UiO-66(3Zr:3Hf) and summarizing crystallinity thresholds across the series. In a relevant study, Redfern et al. attributed the reduced stability of UiO-66(Ce) to the partial reduction of Ce^{4+} to Ce^{3+} in approximately 47% of the metal nodes, weakening Ce-carboxylate coordination and diminishing framework robustness.[126] These results highlight how both metal-node chemistry and coordination connectivity critically influence mechanical resilience in MOFs.

An often-overlooked variable in mechanical tuning is linker functionalization. Depending on their size and interaction with

This journal is © The Royal Society of Chemistry 2025

J. Mater. Chem. A, 2025, 13, 33012–33033 | 33023

Table 1 Experimental and computational values of different moduli found in literature

MOF type	Young modulus E (GPa)	Bulk modulus K (GPa)	Shear modulus G (GPa)	Sources
HKUST-1	3.00–6.00[a]	25.9–41.9[a]	1.00–5.40[b]	102 and 103–105
MOF-5 (IRMOF-1)	2.70 ± 1.00[a]	16.3[b]	3.70–0.30[b]	102, 106 and 107
UiO-66(Zr)	22.0–45.0[a]	39.0[a]	13.75[b]	102, 108 and 109
MOF-808(Zr)	26.9 ± 5.2[a]	15.0[a]	—	108 and 110
NU-1000	21.0 ± 3.90[b]	8.20[a]	—	108
UiO-66(Hf)	30.0–60.0[a]	39.49[b]	14.17[b]	102, 109 and 111
ZIF	3.00–9.00[a]	14.0[a]	1.00–4.00[b]	102 and 112–114
IRMOF-10	0.30–12.70[b]	3.50–9.20[b]	0.10–5.00[b]	115
IRMOF-16	0.10–9.36[b]	5.20–5.74[b]	0.04–3.81[b]	115
MOF-801	44.5–50.78[b]	31.2–34.22[b]	17.6–20.27[b]	115
UiO-67	20.00[b]	17.15[b]	5.69[b]	109 and 111
DUT-48 (large pore)	21.0[b]	12.0[b]	8.70[b]	116 and 117
DUT-46/DUT-47 (large pore)	11.1[b]	8.10[b]	4.40[b]	116 and 117
DUT-49(large pore)	10.8[b]	7.50[b]	4.30[b]	116 and 117
DUT-50(large pore)	7.00[b]	5.40[b]	2.70[b]	116 and 117
DUT-151(large pore)	4.70[b]	4.00[b]	1.80[b]	116 and 117
MIL-101(Cr)	0.00497[b]	1.1 ± 0.9[a]	—	118, 119 and 120
MIL-100(Cr)	—	9.0 ± 0.4[a]	—	118

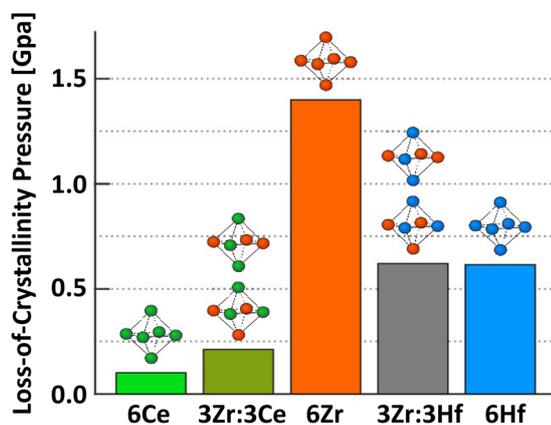[a] Experimental. [b] Computational.

Fig. 12 High-pressure stability of multivariant UiO-66 series. Comparison of crystallinity loss thresholds for mono- and bimetallic UiO-66 materials with different metal centres. Ce-containing frameworks display significantly lower mechanical stability. Adapted from ref. 125 with permission from the American Chemical Society, copyright 2020.

the core linker or metal node, functional groups can significantly influence the rigidity, flexibility, and overall mechanical response of the MOF.[16,102] For instance, Sun *et al.*'s work compared UiO-66 variants bearing bulky –COOH and –F groups against those with smaller –NH$_2$ and –OH substituents, showing that larger groups reinforced the framework *via* hydrogen bonding and steric effects.[102] Marshall *et al.* performed post-synthetic bromination of integral alkyne units within Zr- and Hf-based MOFs.[127] The alkyne units transformed into dibromalkene units, making the linker a little shorter, which caused a 3.7% reduction in pore aperture size. Moosavi *et al.* showed how functional groups like methyl (2-

methylimidazolate), dichloro (dichloroimidazolate), and nitro (2-nitroimidazolate) in ZIFs can create a secondary network of nonbonded interactions referred to as chemical caryatids.[128] Through the incorporation of these chemical caryatids, they effectively reinforced the structure against mechanical stress.

3.3.3 Strategies to mitigate mechanical stress in MOF-based electrolytes. Researchers have increasingly turned to polymer integration strategies to address the inherent brittleness of MOFs while preserving their functional advantages. As discussed in previous subsections, solid-state battery operation involves repeated mechanical stress due to electrode volume fluctuations, which standalone MOFs often struggle to accommodate. Embedding MOFs within polymer matrices or infiltrating MOF pores with polymer chains has emerged as a promising approach to fabricate composite electrolytes with enhanced mechanical resilience. This design can synergistically combine the structural benefits of MOFs – such as intrinsic porosity, ordered ion transport pathways, and tunable chemistry – with the flexibility, elasticity, and stress-dissipation characteristics of polymers. The following examples demonstrate how MOF–polymer hybrids enhance mechanical integrity while also enabling notable improvements in ionic conductivity, electrochemical stability, and interfacial contact.

By infiltrating MOF pores with polymer chains or embedding MOFs within polymer hosts, the mechanical behavior of the composite can be modulated to reflect the flexibility and toughness of the polymeric phase.[129] This hybrid architecture helps the composite withstand the mechanical strains encountered during battery cycling. A representative example is the work by Wang *et al.*, who photopolymerized vinyl-functionalized UiO-66-NH$_2$ with PEGDA and a lithium salt to form a covalently bonded hybrid solid-state polymer electrolyte (HSPE) film.[130] They found that at a MOF : PEGDA ratio of 1 : 8,

this covalently linked network (HSPE-1-8) demonstrated an ionic conductivity of 4.31×10^{-5} S cm^{-1} at 30 °C, more than five times higher than that of PEGDA alone. HSPE-1-8 also maintained low interfacial resistance with lithium metal, attributed to its conformal, stress-dissipating structure that improved mechanical and electrochemical interfacial contact.

Building on this concept, another study incorporated nano-sized UiO-66 particles into a poly(ethylene oxide) (PEO)-based polymer electrolyte.[131] The enhanced performance of the resulting composite was attributed to the coordination between the MOF's metal centers and the ether oxygen atoms in the PEO chains, improving ion transport, as well as the presence of lithium ions doped into the MOF. This composite exhibited an ionic conductivity of 3.0×10^{-5} S cm^{-1} at 25 °C. Additionally, they found that this combination significantly widens the electrochemical window to 4.9 V (*versus* Li$^+$/Li) and improves stability when interfaced with lithium metal anodes. Similarly, Angulakshmi *et al.* developed a PEO-based composite using Mg–BTC as the MOF filler.[132] They reported a significant enhancement in ionic conductivity, ranging from 10^{-5} to 10^{-3} S cm^{-1} between 20 and 70 °C, with the highest values observed in samples containing the lowest weight fraction of PEO.

Expanding the scope beyond lithium systems, Zhang *et al.* introduced polymer chains into the nanopores of ZIF-8 to fabricate a composite electrolyte for sodium metal batteries.[133] This nanoconfinement promoted sodium-ion dissociation and enhanced ion mobility, resulting in an ionic conductivity of 4.01×10^{-4} S cm^{-1}. The electrolyte also exhibited a broadened electrochemical stability window and enabled dendrite-free cycling, retaining 96% of its capacity over 300 cycles.

Wu *et al.* investigated MOF-74 with Cu or Ni metal centers embedded in PEO-based electrolytes for lithium-metal batteries.[134] The Cu-MOF-74 composite achieved a high Young's modulus of 10 GPa and an ionic conductivity of 1.19×10^{-3} S cm^{-1} at 60 °C. In contrast, Ni-MOF-74 did not improve mechanical properties and yielded a lower conductivity of 9.58×10^{-4} S cm^{-1}. The enhanced performance of Cu-MOF-74 was linked to strong hydrogen bonding between its polar functional groups and the PEO matrix, which improved both stress dissipation and ion transport. By comparison, the weaker interactions in the Ni-MOF-74 system led to reduced electrochemical and mechanical performance. These differences are illustrated in Fig. 13, which compares the structural features, mechanical properties, and cycling performance of the two systems.

4 Tuning MOFs to provide optimal ion transport

Structural engineering at the molecular or atomic level is a powerful and increasingly employed strategy to tailor the ion transport properties of MOFs. This section examines how key structural features, such as pore size, dimensionality, and connectivity, influence Li$^+$ mobility. Emphasis is placed on the effects of anisotropic *versus* isotropic transport pathways and the use of biomimetic channel designs to promote directional
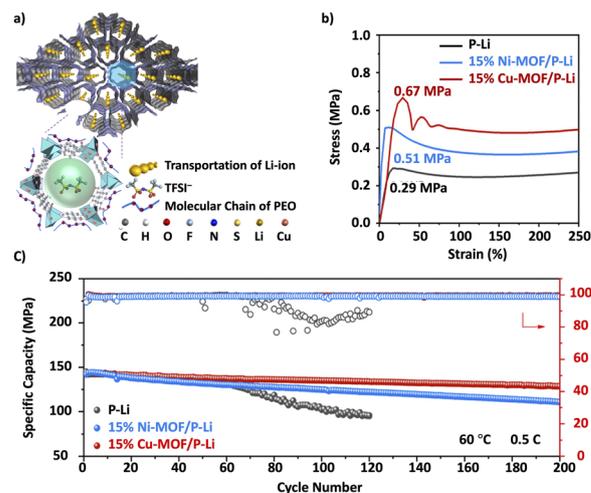

Fig. 13 Structural and electrochemical comparison of MOF-74-based PEO electrolytes with Cu and Ni centers. (a) MOF-74 structure; (b) stress–strain curves showing improved modulus for Cu-MOF/P–Li; (c) cycling performance of symmetric Li cells with different electrolytes at 60 °C. Adapted from ref. 134 with permission from American Chemical Society, copyright 2024.

ion conduction. The section also highlights the impact of defect engineering, where strategies such as introducing missing linkers or open coordination sites can enhance charge carrier density and create additional conduction pathways, though often at the cost of crystallinity. Together, these considerations provide a structure–property design framework for developing MOFs as high-performance ion conductors for next-generation energy storage systems.

4.1 Pore architecture and ion pathways

Ionic conductivity in MOFs is fundamentally governed by the size, shape, and dimensionality of their pore networks. Rational control over these features can enable the formation of continuous ion transport pathways, reduce steric barriers, and enhance ion solvation and mobility.

The coordination geometry of metal nodes defines the overall topology and pore architecture. For example, ZIF-8 features tetrahedrally coordinated Zn^{2+} nodes and imidazolate linkers, forming sodalite-like cages (∼1.1 nm) with narrow pore windows (∼3.4 Å).[135,136] Such narrow apertures can restrict ion diffusion unless assisted by a solvent or salt-anion coordination. On the other hand, many carboxylate MOFs, like UiO-66 (Zr$_6$ nodes) and HKUST-1 (Cu paddlewheels), exhibit larger pore sizes (6–8 Å) that can better accommodate solvated ions.[137,138] Generally, MOFs with more spacious, well-connected channels favor Li$^+$ transport because they reduce steric effects, allowing effective diffusion of the migrating ion.[41,139]

Shen *et al.* demonstrated the critical role of pore size in enhancing Li$^+$ conductivity using Zr-based MOFs. UiO-66 features smaller bicontinuous pores (0.75–1.2 nm), and UiO-67 has larger pores (1.2–2.3 nm).[139] Both MOFs were infiltrated with LiClO$_4$ propylene carbonate (LPC), where ClO$_4^-$ anions anchored to the open metal sites to create biomimetic

This journal is © The Royal Society of Chemistry 2025

J. Mater. Chem. A, 2025, **13**, 33012–33033 | **33025**

ionic channels. The larger-pore UiO-67 (1.2–2.3 nm) exhibited higher ionic conductivity of 6.5×10^{-4} S cm^{-1} and lower activation energy of 0.12 eV than UiO-66 (1.8×10^{-4} S cm^{-1}; 0.21 eV). This enhancement was attributed to reduced confinement effects and more efficient solvation of Li$^+$ ions within the enlarged nanochannels, facilitating faster ion transport across the framework.

However, larger pores are not always advantageous. If the distance between binding sites becomes too large, Li$^+$ hopping may slow down. In this context, Butreddy *et al.* studied a series of isoreticular Li-carboxylate MOFs with increasing linker lengths (BDC: 1,4-benzenedicarboxylic acid, NDC: 1,4-naphthalenedicarboxylic acid, BPDC: 4,4′-biphenyldicarboxylic acid).[41] They found that Li–BPDC, with the smallest pore, yielded the highest conductivity (Fig. 14). The study concluded that excessive pore expansion introduces significant spacing between anchor sites, elevating the activation energy and disrupting efficient ion conduction.

Beyond pore size, the dimensionality and orientation of conduction pathways influence overall transport behavior. MOFs like UiO-66 and MIL-100 possess 3D interconnected networks, enabling isotropic ion conduction that remains effective even in polycrystalline pellets with randomly oriented domains.[137,140,141] In contrast, MOF-74 features one-dimensional channels, which offer high conductivity along the *c*-axis but suffer from reduced performance when crystals are misaligned.[142,143] Hwang *et al.* reported that proton conductivity along the *c*-axis of MOF-74 was over 1200 times greater than in the ab-plane (Fig. 15),[143] while Mirandona-Olaeta later demonstrated that random crystal orientation significantly limited bulk conductivity.[144]

The presence of open metal sites can further enhance ion transport by anchoring anions and creating directed conduction pathways. For example, Shen *et al.*, discussed previously, demonstrated a biomimetic ionic channel by coordinating the perchlorate (ClO$_4^-$) anions of the LiClO$_4$ salt to open Cu sites in HKUST-1, forming negatively charged ion channels that promoted selective Li$^+$ transport.[139] In other words, the
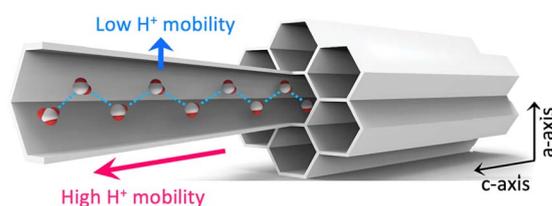

Fig. 15 Schematic illustration of anisotropic proton conduction in MOF-74. One-dimensional hexagonal channels along the *c*-axis enable high H$^+$ mobility, while the orthogonal *a*-axis shows significantly reduced transport. Adapted from ref. 143 with permission from the American Chemical Society, copyright 2018.
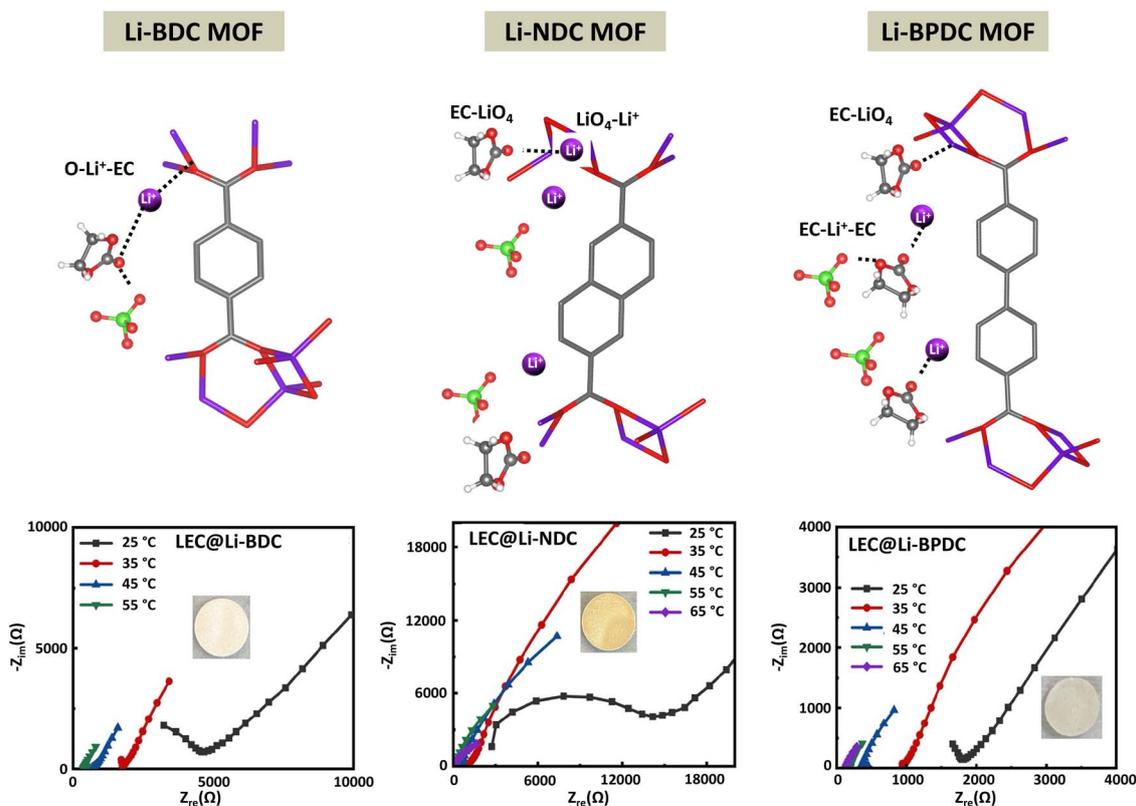
Fig. 14 Li$^+$ conduction behavior in isoreticular Li-carboxylate MOFs featuring benzene (BDC), naphthalene (NDC), and biphenyl (BPDC) linkers. Top: Structural models showing solvation environments and Li$^+$ hopping distances in each MOF. Bottom: Arrhenius plots of ionic conductivity at various temperatures, highlighting that the smallest-pore MOF (Li–BPDC) exhibits the highest conductivity and lowest activation energy. Adapted from ref. 41 with permission from the American Chemical Society, copyright 2023.

33026 | *J. Mater. Chem. A*, 2025, **13**, 33012–33033

This journal is © The Royal Society of Chemistry 2025

framework remains three-dimensional with interconnected pores, but the strategic placement and immobilization of anions create a preferential pathway for Li$^+$ conduction that behaves similarly to a 1D channel. A similar mechanism was observed in the Cu-azolate MOF, MIT-20, where halide or pseudohalide ions bind to Cu centers, rendering the framework anionic and facilitating Li$^+$ accumulation within its hexagonal pores.[68] Park *et al.* reported a dramatic increase in conductivity, from 4.4×10^{-5} to 4.8×10^{-4} S cm^{-1} upon substituting LiBr with LiBF$_4$, attributed to weaker anion–framework interactions that lowered the ion hopping barrier (Fig. 16).[68]

4.2 Defect engineering and functionalization strategies

Defect engineering in MOFs, where lattice imperfections are intentionally introduced, has emerged as a powerful strategy to enhance ionic conductivity. Although such defects often reduce crystallinity, they can simultaneously increase porosity, generate additional charge carriers, and expose new coordination sites that facilitate ion transport. The most common types of defects in MOFs include missing-linker and missing-cluster defects, both of which alter the local electronic and structural environment of the framework.

In zirconium-based MOFs such as UiO-66, the absence of a dicarboxylate linker results in undercoordinated Zr^{4+} centers and a net negative charge on the framework. To maintain charge neutrality, additional cations, such as Li$^+$, can be incorporated, enhancing the density of mobile ions.[145] Early work by Ameloot *et al.* demonstrated this concept by thermally dehydrating UiO-66 to expose Zr sites, followed by grafting lithium *tert*-butoxide (LiOtBu) to cap the vacancies with –OtBu groups and associated Li$^+$ ions (Fig. 17).[145] The resulting material exhibited a room-temperature conductivity of 3.3×10^{-6} S cm^{-1}. Subsequent
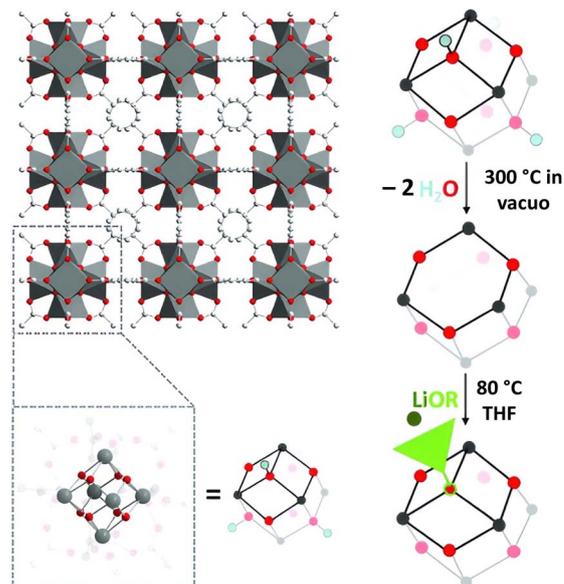

Fig. 17 Post-synthetic modification of UiO-66 to introduce Li$^+$ charge carriers. Dehydration at 300 °C under vacuum generates open Zr sites by removing coordinated water, which are subsequently functionalised with lithium *tert*-butoxide (LiOR) in THF at 80 °C. This results in Li$^+$ incorporation through capping of coordination vacancies. Adapted from ref. 145 with permission from Wiley-VCH, copyright 2013.

work by Yang *et al.* expanded on this strategy by introducing sulfonate-functionalized linkers into UiO-66, effectively converting it into a single-ion conductor.[40] This modification led to a conductivity of approximately 10^{-5} S cm^{-1} at room temperature.[40] Similarly, Wiers *et al.* showed that adding lithium isopropoxide to the open metal sites of Mg$_2$(dobdc) (dobdc$_4^-$ = 1,4-dioxido-2,5-benzenedicarboxylate) produced a Li-MOF solid electrolyte with an ionic conductivity of 3.1×10^{-4} S cm^{-1} at room temperature.[146] Together, these studies highlight how deliberate defect formation and targeted post-synthetic modification can significantly enhance Li$^+$ conductivity in MOFs by increasing the concentration of charge carriers and creating favorable ion transport environments. These strategies offer a robust framework for tuning MOFs as high-performance solid-state electrolytes.

5 Conclusions and outlook

Recent advances have underscored the strong potential of MOFs as solid-state electrolytes, owing to their structural tunability, versatile functionalities, and high porosity. To realize this potential, several strategies have been explored to address critical challenges such as interfacial resistance, mechanical brittleness, and proton interference. This review has identified several key features and persistent challenges that continue to shape the development of MOF-based electrolytes, which are summarized below:

(I) Challenges in accurately measuring ionic conductivity: a central challenge in evaluating MOF-based electrolytes is the interference of protons, often introduced by moisture or other
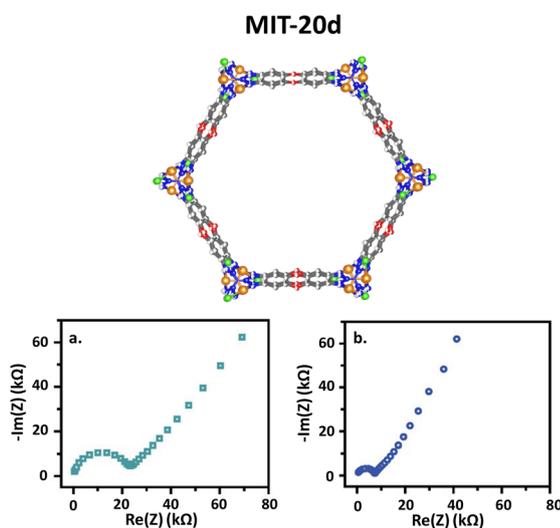
MIT-20d

Fig. 16 Structural and electrochemical characterization of MIT-20d, an anionic Cu-azolate MOF enabling single-ion conduction. (Top) MIT-20d pore structure with open Cu sites coordinating halide anions. Bottom: Nyquist plots of MIT-20-LiCl (a) and MIT-20-LiBr (b), showing improved Li$^+$ conductivity for the latter. Adapted from ref. 68 with permission from the American Chemical Society, copyright 2017.

This journal is © The Royal Society of Chemistry 2025

J. Mater. Chem. A, 2025, **13**, 33012–33033 | **33027**

guest species adsorbed from the environment. Due to their high porosity and often hydrophilic nature, MOFs are prone to absorbing moisture and guest vapors, which can activate unintended conduction pathways, most notably protonic transport. These extrinsic contributions can obscure the underlying ion transport mechanisms, leading to inflated conductivity values, misidentification of the dominant charge carrier, and ambiguity regarding the true solid-state nature of the electrolyte.

This issue underscores the importance of distinguishing between intrinsic and extrinsic ion transport. Intrinsic conductivity in MOFs generally arises from framework-mediated mechanisms, such as single-ion hopping or concerted ion diffusion along well-defined structural pathways. In contrast, extrinsic conduction is typically driven by mobile protons or solvated ions that move through adsorbed water layers or dynamic hydrogen-bond networks, often following Grotthuss- or vehicle-type mechanisms. These mechanistic differences have profound implications not only for interpreting experimental data but also for the rational design of efficient MOF electrolytes.

Moving forward, advancing MOF-based electrolytes will require both precise control of testing environments and in-depth mechanistic analysis of conduction behavior. Mitigating extrinsic effects demands strategies such as performing measurements under rigorously anhydrous conditions, structurally tailoring MOFs to reduce guest molecule uptake, and designing frameworks that promote selective ion transport. At the same time, exploiting framework-embedded pathways presents a promising route to achieving solid-state electrolytes that combine the structural stability of solids with the high ionic mobility characteristic of liquids.

A critical enabler for this progress is the adoption of standardized electrochemical testing protocols. Because MOFs are particularly susceptible to environmental effects and interfacial variability, reproducible ionic conductivity measurements should follow clearly defined and well-reported procedures. For example, reporting fabrication procedures, such as pressing MOF powders into pellets with clearly specified pressure, thickness, and surface preparation parameters, enables meaningful cross-study comparison, regardless of the exact values used. Similarly, the choice of electrode configuration should be justified and documented; symmetric stainless steel (SS|MOF|SS) cells provide a convenient baseline, but Teflon-based or alternative configurations are also widely employed. For Li^+ transport studies, Li|MOF|Li symmetric cells can further evaluate electrochemical stability and transference behavior.

All sample handling should be carried out in an argon-filled glovebox (<1 ppm H_2O and O_2) to avoid moisture-induced proton conduction. The applied stack pressure during testing should be reported and maintained using torque-controlled hardware, as pressure strongly influences interfacial resistance. EIS parameters, including frequency range, AC amplitude, equivalent circuit model, and temperature control, should be consistently documented. By implementing and clearly reporting such standardized methodologies, the community can ensure reliable cross-study comparisons, distinguish

intrinsic MOF conductivity from extrinsic contributions, and accelerate the translation of these materials from laboratory-scale studies to practical solid-state battery applications.

(II) Interfacial contact limitations: robust interfacial contact between MOF electrolytes and electrodes remains a significant bottleneck in solid-state battery integration. MOFs' rigid and brittle morphology often results in poor surface conformity, creating interfacial voids and high resistance "dead zones" that impede ion transport. These issues are exacerbated by mismatches in morphology, particle size, and surface roughness between the electrolyte and electrode materials. To address this, strategies such as incorporating liquid electrolytes, applying mechanical pressure, and fabricating MOF–polymer hybrid membranes have shown promise in enhancing interfacial adhesion and ion transport. Scalable processing techniques like slurry casting and spray-coating also offer practical routes to improved integration, though maintaining uniform distribution and continuous conduction channels remains challenging.

Beyond physical mismatch, chemical reactivity at the electrode–MOF interface under operating conditions presents further complications. Interfacial degradation due to redox reactions, space-charge layer formation, and unstable interfaces can compromise battery performance and lifespan. Mitigation strategies include linker functionalization (e.g., fluorination), polymer blending, and coordination of mobile anions at open metal sites. These techniques can stabilize the interface, suppress undesirable reactions, and preserve ionic conductivity over time.

Mechanical durability is another critical factor, as the brittle nature of most MOFs makes them prone to cracking or fragmentation under the mechanical stress of repeated battery cycling. Strategies such as integrating MOFs into polymeric matrices, employing flexible linkers, optimizing metal–linker connectivity, and incorporating functional groups have proven highly effective in enhancing mechanical stability, flexibility, and resilience.[41,73,91,125,130,131,134,147,148] These design modifications preserve interfacial contact under mechanical strain while retaining the intrinsic porosity and ionic conductivity of the material. These modifications help maintain interfacial contact under strain without sacrificing porosity or conductivity. Future research should continue refining these interfacial design principles, prioritizing integrated solutions that simultaneously address physical, chemical, and mechanical interfacial challenges.

(III) Structural fine-tuning of MOFs for ion transport: the molecular level tunability of MOFs provides a powerful platform for tailoring ion transport mechanisms yet remains underexplored in the development of solid-state electrolytes. Key structural features – including framework topology, pore size and dimensionality, open metal sites, and defect density – have a profound impact on ionic conductivity and can be leveraged to enhance performance. For example, optimizing pore diameters so they are large enough to avoid steric hindrance yet small enough to minimize ion-hopping distances can improve ion transport efficiency. Likewise, the dimensionality of the pore network provides another design lever: three-dimensional pore

33028 | *J. Mater. Chem. A*, 2025, **13**, 33012–33033

This journal is © The Royal Society of Chemistry 2025

networks (*e.g.*, in UiO-66 or MIL-100) support isotropic conduction, while one-dimensional channels (*e.g.*, MOF-74) can achieve directional superionic conductivity when aligned appropriately. Additionally, leveraging open metal sites within MOFs to anchor anions can create biomimetic ion channels that facilitate cation mobility by reducing electrostatic barriers, as demonstrated in $LiClO_4$-loaded HKUST-1 and MIT-20.[68,139] Defect engineering, such as introducing missing linkers or node vacancies, can enhance carrier density and create additional conduction pathways, thereby improving ionic conductivity. However, these benefits often come at the cost of reduced structural stability, as demonstrated in modified UiO-66 and Mg_2(dobdc).[145,146] Future research should adopt a systematic approach to manipulating pore size, defect density, and channel architecture to tailor MOFs' ionic conductivity for next-generation solid-state batteries.

5.1 Emerging opportunities and future directions

As the field of MOF-based solid-state electrolytes advances, several emerging research directions offer promising routes to overcome current limitations and expand the functional capabilities of these materials. Although substantial advances have been made in understanding ion transport mechanisms and interfacial compatibility between electrodes and electrolytes, future breakthroughs will likely depend on the deeper integration of advanced characterization methods, multiscale computational modeling, and interdisciplinary materials design. To ensure these directions are pursued with a rigorous scientific approach, each opportunity below is outlined with its underlying rationale, the specific limitation it addresses, and the methodological pathway for investigation. This section outlines key opportunities expected to drive significant advances in MOF-based electrolytes.

(I) Advanced characterization techniques: understanding ion dynamics and interfacial evolution in MOF-based electrolytes requires real-time, atomic-scale insight. Current *ex situ* characterization fails to capture transient structural changes during cycling. A major frontier involves the development of *in situ* and *operando* tools to probe structural evolution, ion dynamics, and interfacial stability under operating conditions. Techniques such as synchrotron X-ray diffraction, neutron scattering, solid-state NMR, and Raman spectroscopy, when performed *operando*, can reveal changes in framework integrity, coordination environment, and guest–host interactions during cycling.[46,75] Recent work by Cheng *et al.* demonstrated how multi-modal approaches – combining molecular dynamic (MD) simulations, X-ray photoelectron spectroscopy (XPS), NMR, and *operando* cycling tests – can reveal the interplay between structure, ion transport, and interfacial evolution in MOF-based composite electrolytes.[75] Coupling these techniques with impedance spectroscopy and isotope-labeled tracer diffusion can further distinguish between ionic species and elucidate transport mechanisms beyond static conductivity metrics.

(II) Hydrophobic channel integration: preventing water uptake is critical for preserving intrinsic ion transport in humid conditions. Moisture adsorption leads to extrinsic proton conduction that obscures true ionic transport behavior. Incorporating hydrophobic groups into the pore environment reduces affinity for water and polar solvents, preserving intrinsic ion-transport pathways. A compelling example is the fluorinated UiO-66 coating developed by Wang *et al.*[149] The fluorinated framework created a superhydrophobic interface, significantly reducing moisture adsorption, thus minimizing proton conductivity. This example highlights how molecular-level surface modifications can stabilize ionic conduction by blocking moisture interference.

(III) Data-driven MOF design and screening: accelerating discovery requires predictive identification of high-performance candidates. Experimental trial-and-error is slow and resource-intensive. High-throughput computational screening (HTCS) and machine learning (ML) techniques have emerged as powerful tools for accelerating the discovery of MOFs with superior ionic transport properties. Bucior *et al.* pioneered a large-scale screening approach that employed structural descriptors, such as pore size, surface area, and void fraction, to predict performance across thousands of reported and predicted MOFs, primarily for gas adsorption.[150] The same structure–property modeling approach can be extended to ion transport, as the underlying pore architectures and binding site distributions similarly govern ion mobility. Li *et al.* reviewed how ML models, including random forests, support vector machines, and graph neural networks, can be trained on HTCS-generated datasets to predict MOF properties.[151] These frameworks integrate data from molecular simulations (*e.g.*, GCMC and MD) to enable rapid property predictions, bypassing the time- and resource-intensive synthesis test cycles. As databases of reported and predicted MOFs expand, ML-guided pipelines will pinpoint candidates for roles ranging from selective ion sieving to mechanically adaptive conduction. By merging HTCS with ML, the field is shifting from experimental trial-and-error to predictive discovery, enabling rapid selection of MOFs with appropriate porosity, ion hopping sites, and mechanical integrity.

(IV) Multivalent ion conduction: expanding beyond Li^+, MOF electrolytes tailored for multivalent ions (*e.g.*, Mg^{2+}, Zn^{2+}, Ca^{2+}) represent a promising direction for next-generation energy storage systems with higher theoretical energy densities. These ions offer the potential for multiple electron transfers per ion, improving charge capacity, but their strong electrostatic interactions and bulky solvation shells pose substantial diffusion challenges, often resulting in sluggish ion mobility and poor interfacial compatibility in conventional solid-state systems.[152–154] MOFs can overcome these challenges by promoting partial desolvation and stabilizing ion-migration pathways. Notably, MIL-101 has demonstrated superionic Mg^{2+} conductivity, underscoring the viability of MOFs for multivalent transport and their untapped potential in next-generation battery chemistries.[49]

(V) Flexible composites for mechanical stability and scale-up: mechanical fragility remains a significant obstacle to the practical deployment of MOF electrolytes. Hybridizing MOFs with polymers – either by embedding polymers within MOFs or dispersing MOFs in polymer matrices – combines MOFs'

This journal is © The Royal Society of Chemistry 2025

J. Mater. Chem. A, 2025, **13**, 33012–33033 | **33029**

structural integrity and ionic functionalities with the polymer's flexibility and processability. These composites improve interfacial contact, accommodate volume changes, and mitigate crack formation during cycling. Moreover, this approach enables the fabrication of large-area, freestanding membranes, a critical step toward scalable manufacturing. As such, MOF–polymer composites represent one of the most promising routes for transitioning MOF-based electrolytes from lab-scale demonstrations to real-world energy storage devices.

Overall, the future of MOF-based electrolytes will benefit from an integrated approach that unites precision synthesis with advanced characterization, computational insights, and scalable composite design. These emerging directions reinforce the versatility of MOFs as ion-conducting materials and highlight the transformative potential of interdisciplinary research in overcoming performance limitations. By aligning theoretical modelling with experimental validation and practical design, the field is well-positioned to develop solid-state electrolytes that are chemically and mechanically stable, efficient, and adaptable to meet the evolving demands of next-generation energy storage technologies.

Conflicts of interest

There are no conflicts to declare.

Data availability

No primary research data, software, or code have been included, and no new data were generated or analyzed as part of this review.

Acknowledgements

Notes and references

1 Y. Lv, *Front. Energy Res.*, 2023, **11**, 1258044.
2 A. Dhage, *Battery Design from Chemistry to Pack*, 2023.
3 D. Bogdanov, J. Farfan, K. Sadovskaia, A. Aghahosseini, M. Child, A. Gulagi, A. S. Oyewo, L. De Souza Noel Simas Barbosa and C. Breyer, *Nat. Commun.*, 2019, **10**, 1077.
4 S. Tart, M. Groth and P. Seipold, *Climate Services*, 2020, **17**, 100109.
5 F. Degen, M. Winter, D. Bendig and J. Tübke, *Nat. Energy*, 2023, **8**, 1284–1295.
6 C. Wang and X. Sun, *Engineering*, 2023, **21**, 32–35.
7 N. Sarfraz, N. Kanwal, M. Ali, K. Ali, A. Hasnain, M. Ashraf, M. Ayaz, J. Ifthikar, S. Ali, A. Hendi, N. Baig, M. F. Ehsan, S. S. Shah, R. Khan and I. Khan, *Energy Storage Mater.*, 2024, **71**, 103619.
8 O. B. Chae and B. L. Lucht, *Adv. Energy Mater.*, 2023, **13**, 2203791.
9 S. Kalnaus, N. J. Dudney, A. S. Westover, E. Herbert and S. Hackney, *Science*, 2023, **381**, eabg5998.
10 Z. Zhang, X. Wang, X. Li, J. Zhao, G. Liu, W. Yu, X. Dong and J. Wang, *Mater. Today Sustain.*, 2023, **21**, 100316.
11 H. Yang and N. Wu, *Energy Sci. Eng.*, 2022, **10**, 1643–1671.
12 A. Machín, C. Morant and F. Márquez, *Batteries*, 2024, **10**, 29.
13 Q. Zhao, S. Stalin, C.-Z. Zhao and L. A. Archer, *Nat. Rev. Mater.*, 2020, **5**, 229–252.
14 A. Ramasubramanian, V. Yurkiv, T. Foroozan, M. Ragone, R. Shahbazian-Yassar and F. Mashayek, *J. Phys. Chem. C*, 2019, **123**, 10237–10245.
15 M. Liu, C. Wang, C. Zhao, E. Van Der Maas, K. Lin, V. A. Arszelewska, B. Li, S. Ganapathy and M. Wagemaker, *Nat. Commun.*, 2021, **12**, 5943.
16 R. A. Kharod, J. L. Andrews and M. Dincă, *Annu. Rev. Mater. Res.*, 2022, **52**, 103–128.
17 J. W. Fergus, *J. Power Sources*, 2010, **195**, 4554–4569.
18 S. Li, S. Zhang, L. Shen, Q. Liu, J. Ma, W. Lv, Y. He and Q. Yang, *Adv. Sci.*, 2020, **7**, 13088.
19 D. Karabelli, K. P. Birke and M. Weeber, *Batteries*, 2021, **7**, 18.
20 H. Furukawa, K. E. Cordova, M. O'Keeffe and O. M. Yaghi, *Science*, 2013, **341**, 1230444.
21 L. J. Murray, M. Dincă and J. R. Long, *Chem. Soc. Rev.*, 2009, **38**, 1294.
22 H. Furukawa, K. E. Cordova, M. O'Keeffe and O. M. Yaghi, *Science*, 2013, **341**, 1230444.
23 R. Zhao, Y. Wu, Z. Liang, L. Gao, W. Xia, Y. Zhao and R. Zou, *Energy Environ. Sci.*, 2020, **13**, 2386–2403.
24 H. Guo and C. Zhao, *Small Methods*, 2024, **8**, 2300699.
25 M. Sadakiyo, T. Yamada and H. Kitagawa, *J. Am. Chem. Soc.*, 2009, **131**, 9906–9907.
26 R. Mehek, N. Iqbal, T. Noor, M. Z. B. Amjad, G. Ali, K. Vignarooban and M. A. Khan, *RSC Adv.*, 2021, **11**, 29247–29266.
27 D. K. Panda, K. Maity, A. Palukoshka, F. Ibrahim and S. Saha, *ACS Sustainable Chem. Eng.*, 2019, **7**, 4619–4624.
28 J.-F. Wu and X. Guo, *J. Mater. Chem. A*, 2019, **7**, 2653–2659.
29 M. Sadakiyo and H. Kitagawa, *Dalton Trans.*, 2021, **50**, 5385–5397.
30 T. Wei, Z. Wang, Q. Zhang, Y. Zhou, C. Sun, M. Wang, Y. Liu, S. Wang, Z. Yu, X. Qiu, S. Xu and S. Qin, *CrystEngComm*, 2022, **24**, 5014–5030.
31 P. Shewmon, *Diffusion in Solids*, Springer International Publishing, Cham s.l, 2nd edn, 2016.
32 A. L. G. Biancolli, A. Konovalova, E. I. Santiago and S. Holdcroft, *Int. J. Electrochem. Sci.*, 2023, **18**, 100288.
33 R. G. Linford and S. Hackwood, *Chem. Rev.*, 1981, **81**, 327–364.
34 X. He, Y. Zhu and Y. Mo, *Nat. Commun.*, 2017, **8**, 15893.
35 S. Ma, L. Shen, Q. Liu, W. Shi, C. Zhang, F. Liu, J. A. Baucom, D. Zhang, H. Yue, H. B. Wu and Y. Lu, *ACS Appl. Mater. Interfaces*, 2020, **12**, 43824–43832.
36 K. Otake and H. Kitagawa, *Small*, 2021, **17**, 2006189.
37 K. Kreuer, A. Rabenau and W. Weppner, *Angew Chem. Int. Ed. Engl.*, 1982, **21**, 208–209.

33030 | *J. Mater. Chem. A*, 2025, **13**, 33012–33033

This journal is © The Royal Society of Chemistry 2025

38 P. Ramaswamy, N. E. Wong and G. K. H. Shimizu, *Chem. Soc. Rev.*, 2014, **43**, 5913–5932.

39 N. Agmon, *Chem. Phys. Lett.*, 1995, **244**, 456–462.

40 H. Yang, B. Liu, J. Bright, S. Kasani, J. Yang, X. Zhang and N. Wu, *ACS Appl. Energy Mater.*, 2020, **3**, 4007–4013.

41 P. Butreddy, M. Wijesingha, S. Laws, G. Pathiraja, Y. Mo and H. Rathnayake, *Chem. Mater.*, 2023, **35**, 9857–9878.

42 T. Famprikis, P. Canepa, J. A. Dawson, M. S. Islam and C. Masquelier, *Nat. Mater.*, 2019, **18**, 1278–1291.

43 C. López, R. Rurali and C. Cazorla, *J. Am. Chem. Soc.*, 2024, **146**, 8269–8279.

44 T. Hou, W. Xu, X. Pei, L. Jiang, O. M. Yaghi and K. A. Persson, *J. Am. Chem. Soc.*, 2022, **144**, 13446–13450.

45 J. Brus, J. Czernek, M. Urbanova, J. Rohlíček and T. Plecháček, *ACS Appl. Mater. Interfaces*, 2020, **12**, 47447–47456.

46 M. K. Sarango-Ramírez, M. Donoshita, Y. Yoshida, D. Lim and H. Kitagawa, *Angew. Chem., Int. Ed.*, 2023, **62**, e202301284.

47 L. S. Xie, G. Skorupskii and M. Dincă, *Chem. Rev.*, 2020, **120**, 8536–8580.

48 Y. Wang, P. S. Brodale, X. Miao, C. H. Hendon and L. Sun, *Commun. Mater.*, 2024, **5**, 172.

49 Y. Yoshida, T. Yamada, Y. Jing, T. Toyao, K. Shimizu and M. Sadakiyo, *J. Am. Chem. Soc.*, 2022, **144**, 8669–8675.

50 A. Ulihin, V. Ponomareva, N. Uvarov, K. Kovalenko and V. Fedin, *Ionics*, 2020, **26**, 6167–6173.

51 V. Nozari, C. Calahoo, J. M. Tuffnell, P. Adelhelm, K. Wondraczek, S. E. Dutton, T. D. Bennett and L. Wondraczek, *Sci. Rep.*, 2020, **10**, 3532.

52 R. Chen, Q. Li, X. Yu, L. Chen and H. Li, *Chem. Rev.*, 2020, **120**, 6820–6877.

53 A. Banerjee, X. Wang, C. Fang, E. A. Wu and Y. S. Meng, *Chem. Rev.*, 2020, **120**, 6878–6933.

54 K. Kerman, A. Luntz, V. Viswanathan, Y.-M. Chiang and Z. Chen, *J. Electrochem. Soc.*, 2017, **164**, A1731–A1744.

55 J. Janek and W. G. Zeier, *Nat. Energy*, 2016, **1**, 16141.

56 G. Lu, G. Meng, Q. Liu, L. Feng, J. Luo, X. Liu, Y. Luo and P. K. Chu, *Adv. Powder Mater.*, 2024, **3**, 100154.

57 J. Wang, I. Imaz and D. Maspoch, *Small Struct.*, 2022, **3**, 2100126.

58 Z. Sun, M. Liu, Y. Zhu, R. Xu, Z. Chen, P. Zhang, Z. Lu, P. Wang and C. Wang, *Sustainability*, 2022, **14**, 9090.

59 W. Lyu, H. Fu, A. M. Rao, Z. Lu, X. Yu, Y. Lin, J. Zhou and B. Lu, *Sci. Adv.*, 2024, **10**, eadr9602.

60 B. Hennequart, M. Platonova, R. Chometon, T. Marchandier, A. Benedetto, E. Quemin, R. Dugas, C. Lethien and J.-M. Tarascon, *ACS Energy Lett.*, 2024, **9**, 454–460.

61 Y. Yan, C. Wang, Z. Cai, X. Wang and F. Xuan, *ACS Appl. Mater. Interfaces*, 2023, **15**, 42845–42853.

62 R. Lin, J. Hou, M. Li, Z. Wang, L. Ge, S. Li, S. Smart, Z. Zhu, T. D. Bennett and V. Chen, *Chem. Commun.*, 2020, **56**, 3609–3612.

63 M. I. Nandasiri, S. R. Jambovane, B. P. McGrail, H. T. Schaef and S. K. Nune, *Coord. Chem. Rev.*, 2016, **311**, 38–52.

64 F. Ghamari, D. Raoufi, J. Arjomandi and D. Nematollahi, *Colloids Surf., A*, 2023, **656**, 130450.

65 B. Wang, J. Ke, H. Huang, P. Ren and J. Zhang, *ACS Appl. Mater. Interfaces*, 2025, **17**, 2666–2677.

66 A. I. O. Zaid, *Int. J. Theor. Appl. Mech.*, 2016, **1**, 155–164.

67 M. Da Silva and J. Rajchenbach, *Nature*, 2000, **406**, 708–710.

68 S. S. Park, Y. Tulchinsky and M. Dincă, *J. Am. Chem. Soc.*, 2017, **139**, 13260–13263.

69 C. J. Felice, G. R. Ruiz, R. E. Madrid and M. E. Valentinuzzi, in *Proceedings of the Second Joint 24th Annual Conference and the Annual Fall Meeting of the Biomedical Engineering Society] [Engineering in Medicine and Biology*, IEEE, Houston, TX, USA, 2002, vol. 2, pp. 1677–1678.

70 K. Titov, Z. Zeng, M. R. Ryder, A. K. Chaudhari, B. Civalleri, C. S. Kelley, M. D. Frogley, G. Cinque and J.-C. Tan, *J. Phys. Chem. Lett.*, 2017, **8**, 5035–5040.

71 Surface roughness of ventilation ducts, *The Engineering Toolbox*, **https://www.engineeringtoolbox.com/surface-roughness-ventilation-ducts-d_209.html**, accessed 12 April 2025.

72 M. Farina, B. B. Duff, C. Tealdi, A. Pugliese, F. Blanc and E. Quartarone, *ACS Appl. Mater. Interfaces*, 2021, **13**, 53986–53995.

73 A. U. Ortiz, A. Boutin, K. J. Gagnon, A. Clearfield and F.-X. Coudert, *J. Am. Chem. Soc.*, 2014, **136**, 11540–11545.

74 J. Guan, X. Feng, Q. Zeng, Z. Li, Y. Liu, A. Chen, H. Wang, W. Cui, W. Liu and L. Zhang, *Adv. Sci.*, 2023, **10**, 2203916.

75 P. Cheng, S. Liu, X. Jia, Y. Jiang and X. Zhang, *Nano Lett.*, 2025, **25**, 6152–6159.

76 X. Wang, B. Pang, L. Kong, Y. Zhu, C. Chen, H. Dong, L. Yu and L. Dong, *J. Appl. Polym. Sci.*, 2025, **142**, e56780.

77 S. Fischer, J. Roeser, T. C. Lin, R. H. DeBlock, J. Lau, B. S. Dunn, F. Hoffmann, M. Fröba, A. Thomas and S. H. Tolbert, *Angew. Chem., Int. Ed.*, 2018, **57**, 16683–16687.

78 Z. Li, S. Wang, J. Shi, Y. Liu, S. Zheng, H. Zou, Y. Chen, W. Kuang, K. Ding, L. Chen, Y. Lan, Y. Cai and Q. Zheng, *Energy Storage Mater.*, 2022, **47**, 262–270.

79 S. Jiang, T. Lv, Y. Peng and H. Pang, *Adv. Sci.*, 2023, **10**, 2206887.

80 M. F. Majid, H. F. Mohd Zaid, C. F. Kait, A. Ahmad and K. Jumbri, *Nanomaterials*, 2022, **12**, 1076.

81 O. K. Farha, I. Eryazici, N. C. Jeong, B. G. Hauser, C. E. Wilmer, A. A. Sarjeant, R. Q. Snurr, S. T. Nguyen, A. Ö. Yazaydın and J. T. Hupp, *J. Am. Chem. Soc.*, 2012, **134**, 15016–15021.

82 Z. Cheng, M. Liu, S. Ganapathy, C. Li, Z. Li, X. Zhang, P. He, H. Zhou and M. Wagemaker, *Joule*, 2020, **4**, 1311–1323.

83 H. Zhu, S. Li, L. Peng, W. Zhong, Q. Wu, S. Cheng and J. Xie, *Nano Energy*, 2024, **125**, 109571.

84 Y. Li, J.-T. Han, C.-A. Wang, H. Xie and J. B. Goodenough, *J. Mater. Chem.*, 2012, **22**, 15357.

85 Z. Zhang, J. Gou, K. Cui, X. Zhang, Y. Yao, S. Wang and H. Wang, *Nano-Micro Lett.*, 2024, **16**, 181.

86 Y.-S. Choi and J.-C. Lee, *J. Power Sources*, 2019, **415**, 189–196.

This journal is © The Royal Society of Chemistry 2025

J. Mater. Chem. A, 2025, **13**, 33012–33033 | **33031**

87 S. Cao, Z. Xu, W. Shi, Z. Dai, Z. Fu, F. Chen, Q. Shen and L. Zhang, *ACS Appl. Mater. Interfaces*, 2025, **17**, 16758–16767.

88 C. Xiao, X. Liu, W. Li, X. Ma, J. Qian and X. Lin, *Batteries*, 2024, 7, e202400078.

89 P. Dong, X. Zhang, W. Hiscox, J. Liu, J. Zamora, X. Li, M. Su, Q. Zhang, X. Guo, J. McCloy and M. Song, *Adv. Mater.*, 2023, **35**, 2211841.

90 A. U. Mu, G. Cai and Z. Chen, *Adv. Sci.*, 2024, **11**, 2305280.

91 J. Li, F. Xie, W. Pang, Q. Liang, X. Yang and L. Zhang, *Sci. Adv.*, 2024, **10**, eadl3925.

92 P.-A. Le, N. T. Nguyen, P. L. Nguyen, T. V. B. Phung and C. D. Do, *Heliyon*, 2023, **9**, e19746.

93 M. Li, S. Yang and B. Li, *Interdiscip. Mater.*, 2024, **3**, 805–834.

94 K. Lee, E. Kazyak, M. J. Wang, N. P. Dasgupta and J. Sakamoto, *Joule*, 2022, **6**, 2547–2565.

95 Z. Wang, R. Tan, H. Wang, L. Yang, J. Hu, H. Chen and F. Pan, *Adv. Mater.*, 2018, **30**, 1704436.

96 L. He, Z. Di, J. Li, S. Wang, W. Kong, R. Li, A. Proskurin, C. Lv and T. Wei, *Chem. Commun.*, 2024, **60**, 14637–14640.

97 Z. Hong, P. Li, Q. Zou, L. Gu, J. Wang, L. Deng, C. Wang, Y. Zhang, M. Li, J. Chen, R. Si and C. Yang, *ACS Appl. Energy Mater.*, 2024, **7**, 11967–11976.

98 T. H. Lee, B. K. Lee, S. Y. Yoo, H. Lee, W.-N. Wu, Z. P. Smith and H. B. Park, *Nat. Commun.*, 2023, **14**, 8330.

99 J. Gao, Y. Chai, J. Ni, Y. Zeng, G. Zhang, X. Liu, D. Ning, X. Jin, H. Zhao, D. Zhou, R. Gao, W. Wu, J. Wang and Y. Li, *Chem. Eng. J.*, 2025, **512**, 162738.

100 W. Tian, G. Lin, S. Yuan, T. Jin, Q. Wang and L. Jiao, *Angew. Chem., Int. Ed.*, 2025, **64**, e202423075.

101 *Mechanical Behaviour of Metal – Organic Framework Materials*, ed. J.-C. Tan, The Royal Society of Chemistry, 1st edn, 2023.

102 Y. Sun, Z. Hu, D. Zhao and K. Zeng, *ACS Appl. Mater. Interfaces*, 2017, **9**, 32202–32210.

103 A. K. Chaudhari, I. Han and J. Tan, *Adv. Mater.*, 2015, **27**, 4438–4446.

104 L. R. Redfern and O. K. Farha, *Chem. Sci.*, 2019, **10**, 10666–10679.

105 M. R. Ryder, B. Civalleri, G. Cinque and J.-C. Tan, *CrystEngComm*, 2016, **18**, 4303–4312.

106 D. F. Bahr, J. A. Reid, W. M. Mook, C. A. Bauer, R. Stumpf, A. J. Skulan, N. R. Moody, B. A. Simmons, M. M. Shindel and M. D. Allendorf, *Phys. Rev. B:Condens. Matter Mater. Phys.*, 2007, **76**, 184106.

107 H. Jiang, S. M. Moosavi, J. Czaban-Jóźwiak, B. Torre, A. Shkurenko, Z. O. Ameur, J. Jia, N. Alsadun, O. Shekhah, E. Di Fabrizio, B. Smit and M. Eddaoudi, *Matter*, 2023, **6**, 285–295.

108 G. P. Robertson, S. Mosca, C. Castillo-Blas, F. A. Son, O. K. Farha, D. A. Keen, S. Anzellini and T. D. Bennett, *Inorg. Chem.*, 2023, **62**, 10092–10099.

109 H. Wu, T. Yildirim and W. Zhou, *J. Phys. Chem. Lett.*, 2013, **4**, 925–930.

110 Z. Hu, T. Kundu, Y. Wang, Y. Sun, K. Zeng and D. Zhao, *ACS Sustainable Chem. Eng.*, 2020, **8**, 17042–17053.

111 Z. Wang, K. M. Schmalbach, R. L. Combs, Y. Chen, R. L. Penn, N. A. Mara and A. Stein, *ACS Appl. Mater. Interfaces*, 2020, **12**, 49971–49981.

112 J. C. Tan, T. D. Bennett and A. K. Cheetham, *Proc. Natl. Acad. Sci. U. S. A.*, 2010, **107**, 9938–9943.

113 E. C. Spencer, R. J. Angel, N. L. Ross, B. E. Hanson and J. A. K. Howard, *J. Am. Chem. Soc.*, 2009, **131**, 4022–4026.

114 B. Zheng, Y. Zhu, F. Fu, L. L. Wang, J. Wang and H. Du, *RSC Adv.*, 2017, **7**, 41499–41503.

115 K. Banlusan and A. Strachan, *J. Chem. Phys.*, 2017, **146**, 184705.

116 S. Krause, J. D. Evans, V. Bon, I. Senkovska, P. Iacomi, F. Kolbe, S. Ehrling, E. Troschke, J. Getzschmann, D. M. Többens, A. Franz, D. Wallacher, P. G. Yot, G. Maurin, E. Brunner, P. L. Llewellyn, F.-X. Coudert and S. Kaskel, *Nat. Commun.*, 2019, **10**, 3632.

117 P. Ying, J. Zhang and Z. Zhong, *J. Phys. Chem. C*, 2021, **125**, 12991–13001.

118 A. Celeste, P. Fertey, J.-P. Itié, G. Blanita, C. Zlotea and F. Capitani, *J. Am. Chem. Soc.*, 2024, **146**, 9155–9162.

119 A. Celeste, F. Capitani, P. Fertey, A. Paolone, F. Borondics, O. Grad, G. Blanita and C. Zlotea, *ACS Appl. Nano Mater.*, 2022, **5**, 4196–4203.

120 B. B. Shah, T. Kundu and D. Zhao, *Top. Curr. Chem.*, 2019, **377**, 25.

121 T. R. Garrick, X. Huang, V. Srinivasan and J. W. Weidner, *J. Electrochem. Soc.*, 2017, **164**, E3552–E3558.

122 P. M. Gomadam and J. W. Weidner, *J. Electrochem. Soc.*, 2006, **153**, A179.

123 H. He, N. Deng, X. Wang, L. Gao, C. Tang, E. Wu, J. Ren, X. Yang, N. Feng, D. Gao and X. Zhuang, *Adv. Funct. Mater.*, 2025, 2421670.

124 X. Song, X. Liu, M. Oh and M. S. Lah, *Cryst. Growth Des.*, 2010, **10**, 3222–3227.

125 S. M. J. Rogge, P. G. Yot, J. Jacobsen, F. Muniz-Miranda, S. Vandenbrande, J. Gosch, V. Ortiz, I. E. Collings, S. Devautour-Vinot, G. Maurin, N. Stock and V. Van Speybroeck, *ACS Mater. Lett.*, 2020, **2**, 438–445.

126 L. R. Redfern, M. Ducamp, M. C. Wasson, L. Robison, F. A. Son, F.-X. Coudert and O. K. Farha, *Chem. Mater.*, 2020, **32**, 5864–5871.

127 R. J. Marshall, S. L. Griffin, C. Wilson and R. S. Forgan, *J. Am. Chem. Soc.*, 2015, **137**, 9527–9530.

128 S. M. Moosavi, P. G. Boyd, L. Sarkisov and B. Smit, *ACS Cent. Sci.*, 2018, **4**, 832–839.

129 T. Iizuka, N. Hosono and T. Uemura, *Dalton Trans.*, 2022, **51**, 13204–13209.

130 Z. Wang, S. Wang, A. Wang, X. Liu, J. Chen, Q. Zeng, L. Zhang, W. Liu and L. Zhang, *J. Mater. Chem. A*, 2018, **6**, 17227–17234.

131 F. Liang and Z. Wen, *J. Inorg. Mater.*, 2021, **36**, 332.

132 N. Angulakshmi, R. S. Kumar, M. A. Kulandainathan and A. M. Stephan, *J. Phys. Chem. C*, 2014, **118**, 24240–24247.

133 J. Zhang, Y. Wang, Q. Xia, X. Li, B. Liu, T. Hu, M. Tebyetekerwa, S. Hu, R. Knibbe and S. Chou, *Angew. Chem.*, 2024, **136**, e202318822.

33032 | *J. Mater. Chem. A*, 2025, **13**, 33012–33033

This journal is © The Royal Society of Chemistry 2025

134 J. Wu, Y. Ma, H. Zhang, H. Xie, J. Hu, C. Shi, B. Chen, C. He and N. Zhao, *ACS Appl. Mater. Interfaces*, 2024, **16**, 16351–16362.

135 J. Zhao, R. Fan, S. Xiang, J. Hu and X. Zheng, *Membranes*, 2023, **13**, 500.

136 L. Tian, Z. Liu, F. Tao, M. Liu and Z. Liu, *Dalton Trans.*, 2021, **50**, 13877–13882.

137 V. G. Ponomareva, E. S. Shutova, K. A. Kovalenko and V. P. Fedin, *Molecules*, 2022, **27**, 8387.

138 T. Zelenka, M. Baláž, M. Férová, P. Diko, J. Bednarčík, A. Királyová, Ľ. Zauška, R. Bureš, P. Sharda, N. Király, A. Badač, J. Vyhlídalová, M. Želinská and M. Almáši, *Sci. Rep.*, 2024, **14**, 15386.

139 L. Shen, H. B. Wu, F. Liu, J. L. Brosmer, G. Shen, X. Wang, J. I. Zink, Q. Xiao, M. Cai, G. Wang, Y. Lu and B. Dunn, *Adv. Mater.*, 2018, **30**, 1707476.

140 M. Islamov, P. Boone, H. Babaei, A. J. H. McGaughey and C. E. Wilmer, *Chem. Sci.*, 2023, **14**, 6592–6600.

141 M.-L. Chen, S.-Y. Zhou, Z. Xu, L. Ding and Y.-H. Cheng, *Molecules*, 2019, **24**, 3718.

142 D. Britt, H. Furukawa, B. Wang, T. G. Glover and O. M. Yaghi, *Proc. Natl. Acad. Sci. U. S. A.*, 2009, **106**, 20637–20640.

143 S. Hwang, E. J. Lee, D. Song and N. C. Jeong, *ACS Appl. Mater. Interfaces*, 2018, **10**, 35354–35360.

144 A. Mirandona-Olaeta, E. Goikolea, S. Lanceros-Mendez, A. Fidalgo-Marijuan and I. Ruiz De Larramendi, *Batteries*, 2024, **10**, 203.

145 R. Ameloot, M. Aubrey, B. M. Wiers, A. P. Gómora-Figueroa, S. N. Patel, N. P. Balsara and J. R. Long, *Chem.–Eur. J.*, 2013, **19**, 5533–5536.

146 B. M. Wiers, M.-L. Foo, N. P. Balsara and J. R. Long, *J. Am. Chem. Soc.*, 2011, **133**, 14522–14525.

147 J. Zhou, X. Wang, J. Fu, L. Chen, X. Wei, R. Jia and L. Shi, *Small*, 2024, **20**, 2309317.

148 V. V. Karve, A. Neves Vieira, D. Stoian, O. Trukhina and W. L. Queen, *Chem. Commun.*, 2022, **58**, 11559–11562.

149 Z. Wang, P. Wang, J. Zhang, X. Yang, X. Wu, W. Duan, Y. Yue, J. Xie, Y. Liu and H. Tian, *J. Power Sources*, 2024, **622**, 235364.

150 B. J. Bucior, A. S. Rosen, M. Haranczyk, Z. Yao, M. E. Ziebel, O. K. Farha, J. T. Hupp, J. I. Siepmann, A. Aspuru-Guzik and R. Q. Snurr, *Cryst. Growth Des.*, 2019, **19**, 6682–6697.

151 C. Li, L. Bao, Y. Ji, Z. Tian, M. Cui, Y. Shi, Z. Zhao and X. Wang, *Coord. Chem. Rev.*, 2024, **514**, 215888.

152 Y. Zhan, W. Zhang, B. Lei, H. Liu and W. Li, *Front. Chem.*, 2020, **8**, 125.

153 J. Luo, Y. Li, H. Zhang, A. Wang, W. Lo, Q. Dong, N. Wong, C. Povinelli, Y. Shao, S. Chereddy, S. Wunder, U. Mohanty, C. Tsung and D. Wang, *Angew. Chem., Int. Ed.*, 2019, **58**, 15313–15317.

154 Z. Rong, R. Malik, P. Canepa, G. Sai Gautam, M. Liu, A. Jain, K. Persson and G. Ceder, *Chem. Mater.*, 2015, **27**, 6016–6021.

This journal is © The Royal Society of Chemistry 2025

J. Mater. Chem. A, 2025, **13**, 33012–33033 | **33033**